Improved rain rate and drop size retrievals from airborne Doppler radar

Atmos. Chem. Phys., 17, 11567–11589, 2017
https://doi.org/10.5194/acp-17-11567-2017

Atmospheric Chemistry and Physics
Open Access
EGU

Improved rain rate and drop size retrievals from airborne Doppler radar

Shannon L. Mason[1,2], **J. Christine Chiu**[1,2], **Robin J. Hogan**[1,3], **and Lin Tian**[4,5]

[1]Department of Meteorology, University of Reading, Reading, UK
[2]National Centre for Earth Observation, University of Reading, Reading, UK
[3]European Centre for Medium-Range Weather Forecasts, Reading, UK
[4]NASA Goddard Space Flight Center, Greenbelt, MD, USA
[5]Morgan State University, Baltimore, MD, USA

Correspondence to: Shannon L. Mason (s.l.mason@reading.ac.uk)

Received: 26 March 2017 – Discussion started: 12 April 2017
Revised: 6 July 2017 – Accepted: 30 August 2017 – Published: 27 September 2017

Abstract. Satellite remote sensing of rain is important for quantifying the hydrological cycle, atmospheric energy budget, and cloud and precipitation processes; however, radar retrievals of rain rate are sensitive to assumptions about the raindrop size distribution. The upcoming EarthCARE satellite will feature a 94 GHz Doppler radar alongside lidar and radiometer instruments, presenting opportunities for enhanced retrievals of the raindrop size distribution.

We demonstrate the capability to retrieve rain rate as a function of drop size and drop number concentration from airborne 94 GHz Doppler radar measurements using CAPTIVATE, the variational retrieval algorithm developed for EarthCARE. For a range of rain regimes observed during the Tropical Composition, Cloud and Climate Coupling field campaign, we explore the contributions of mean Doppler velocity and path-integrated attenuation (PIA) measurements to the retrieval of rain rate, and the retrievals are evaluated against independent measurements from an independent 9.6 GHz Doppler radar. The retrieved drop number concentrations vary over 5 orders of magnitude between very light rain from melting ice and warm rain from liquid clouds. In light rain conditions mean Doppler velocity facilitates estimates of rain rate without PIA, suggesting the possibility of EarthCARE rain rate estimates over land; in moderate warm rain, drop number concentration can be retrieved without mean Doppler velocity, with possible applications to CloudSat.

1 Introduction

Satellite remote sensing of rain is important for quantifying the global water and energy cycles. Even light rain and drizzle make significant contributions to global precipitation at the surface (Haynes et al., 2009; Berg et al., 2010; Behrangi et al., 2012), while the vertical profile of precipitation can be used to estimate the transfer of latent heat (Nelson et al., 2016) and microphysical processes (Lebsock et al., 2013; Wood et al., 2009). The intensity and drop size distribution (DSD) of rain are subject to persistent errors in weather and climate models, which frequently produce excess drizzle from shallow maritime clouds (Stephens et al., 2010; Abel and Boutle, 2012). Improved instrumentation and retrieval algorithms for the satellite remote sensing of rain are therefore priorities for earth observation, model evaluation, and an understanding of cloud and precipitation processes.

The first space-borne cloud and precipitation radars facilitated significant advances in the detection and measurement of rain, especially over the oceans. The 14 GHz precipitation radar aboard the tropical rainfall measurement mission (TRMM; Kummerow et al., 1998) measured moderate and heavy precipitation in the tropics. The more sensitive 94 GHz cloud-profiling radar aboard CloudSat (Stephens et al., 2002) is capable of measuring light rainfall not detected by TRMM, which is very frequent and amounts to 10 % of total tropical maritime precipitation (Berg et al., 2010). CloudSat measurements suggest that around 70 % of marine precipitation

falls as drizzle, 50 to 80 % of which evaporates before reaching the surface (Rapp et al., 2013). The high sensitivity of 94 GHz radar allows for profiling measurements of light rain and drizzle at the cost of significant attenuation in moderate to heavy rain.

The retrieval of rain rate from profiles of apparent radar reflectivity requires knowledge of the attenuation of the radar beam. The path-integrated attenuation (PIA) can be estimated from the ocean surface backscatter relative to nearby clear-sky profiles (Meneghini et al., 1983) or calculated from sea surface wind speed and temperature (Haynes et al., 2009). Estimates of PIA are used in the rain retrieval algorithms of both TRMM (Iguchi et al., 2000; Meneghini and Liao, 2000) and CloudSat (L'Ecuyer and Stephens, 2002; Haynes et al., 2009; Lebsock and L'Ecuyer, 2011) over the ocean; however, the surface backscatter over the land is much more variable and difficult to characterise. Consequently, operational CloudSat data products currently provide only rain detection over land and not rain rate estimates (e.g. Haynes et al., 2009; Lebsock and L'Ecuyer, 2011). Additional radar measurements that facilitate rain rate estimates over land would offer a significant improvement over existing satellite capabilities.

Estimates of rain rate from limited measurements rely upon assumptions about the rain DSD. While the statistical properties of rain DSDs are broadly consistent over time whether measured in situ (Marshall and Palmer, 1948; Tokay and Short, 1996) or estimated by radar remote sensing (Wilson et al., 1997; Illingworth and Blackman, 2002), the instantaneous microphysical properties of rain are observed to vary over many orders of magnitude (Testud et al., 2001). Assumptions about the drop number concentration in particular have been identified as a major source of uncertainty in TRMM and CloudSat estimates of rain rate (Iguchi et al., 2009; Lebsock and L'Ecuyer, 2011). To improve upon the uncertainties of satellite remote-sensed rain rate, there is a need for additional radar measurements with which to better characterize the rain DSD.

Two approaches have been made to improve rain retrievals with additional observations from satellite radars, both to assist in estimating rain rate over land and to better constrain the rain DSD. The recent global precipitation measurement mission (GPM; Hou et al., 2014), with the first dual-frequency radar in space, aims to exploit differences in non-Rayleigh scattering at 35 and 14 GHz to better constrain the rain DSD over land and ocean (e.g. Rose and Chandrasekar, 2006). Another approach is to use Doppler radar to measure the reflectivity-weighted terminal fall speed of raindrops, which relates to drop size. The Doppler spectrum has been used in ground-based radar retrievals to resolve vertical air motion (Atlas et al., 1973; Firda et al., 1999; O'Connor et al., 2005), distinguish cloud from precipitation (Frisch et al., 1995; Luke and Kollias, 2013), and to understand warm rain processes (Kollias et al., 2011b, a). Unfortunately in space-borne radar applications, the Doppler spectrum is broadened by the lateral motion of the radar platform with respect to the scattering hydrometeors (Illingworth et al., 2015), which distorts the higher moments of the Doppler spectrum; consequently, only radar reflectivity, PIA, and mean Doppler velocity measurements are useful for space-borne Doppler radar retrievals.

The upcoming EarthCARE satellite will observe clouds, aerosols, and precipitation using the synergy of 94 GHz Doppler radar, lidar, and radiometers (Illingworth et al., 2015). In this study we use a variational retrieval methodology developed for EarthCARE to investigate improved estimates of rain rate by exploiting mean Doppler velocity measurements to retrieve drop size and drop number concentration parameters of the DSD. NASA's high-altitude ER-2 aircraft provides an ideal platform for testing satellite instruments and retrievals; we use ER-2 measurements taken during the Tropical Composition, Clouds and Climate Coupling field campaign (TC4) off Costa Rica and Panama in 2007 (Toon et al., 2010). A second 9.6 GHz Doppler radar aboard ER-2 provides independent measurements at a less attenuated wavelength, against which the retrievals are evaluated.

The structure of this paper is as follows: we first describe the aircraft measurements, the synergistic classification of hydrometeors, and the retrieval method (Sect. 2). The ambiguities of retrieving rain rate from attenuated radar profiles are discussed using synthetic measurements (Sect. 3) before 94 GHz radar retrievals of rain rate and drop number concentration are presented for three case studies, and the retrievals are evaluated against independent radar measurements (Sect. 4). We briefly consider applications of the retrieval framework to dual-frequency radar retrievals (Sect. 5) and the retrieval of more complex variations in the DSD through the vertical profile (Sect. 6) before summarizing our key findings with a view to applications to EarthCARE retrievals (Sect. 7).

2 Data and retrieval methodology

2.1 Measurements used in the retrieval

The observations are from NASA's high-altitude ER-2 aircraft during the TC4 experiment conducted over the tropical eastern Pacific in July and August 2007 (Toon et al., 2010). ER-2 flies above the tropopause at an altitude of 20 km with a cruise speed of around 200 m s^{-1}. We analyse measurements from straight flight legs over the ocean and average all measurements over 5 s intervals so that each pixel of radar–lidar data has a 1 km along-track footprint.

The 94 GHz (3.2 mm wavelength) cloud radar system (CRS; Li et al., 2004) and 9.6 GHz (3.1 cm wavelength) ER-2 Doppler radar (EDOP; Heymsfield et al., 1996) measure the radar reflectivity factor and mean Doppler velocity with a vertical gate spacing of 37.5 m. The 94 GHz radar reflectivity factor is calibrated against the 9.6 GHz radar near the cloud

top (McGill, 2004), and the mean Doppler velocity measurements are calibrated using the surface signal (Li et al., 2004). The path-integrated attenuation (PIA) of the 94 GHz radar is estimated over the ocean using the surface reference technique (L'Ecuyer and Stephens, 2002; Lebsock and L'Ecuyer, 2011). In this study we focus on the retrieval of rain from the 94 GHz cloud radar and use the 9.6 GHz radar primarily for evaluation.

The cloud physics lidar (CPL; McGill et al., 2002) measures attenuated backscatter at 355, 532, and 1064 nm with the linear polarization ratio measured at the 1064 nm wavelength. In this study the 532 nm attenuated backscatter is used in the classification scheme to detect cloud top and to retrieve overlying ice cloud and liquid layers.

The MODIS airborne simulator (MAS; King et al., 1996) and MODIS/ASTER airborne simulator (MASTER; Hook et al., 2001) imaging radiometers measure infrared (IR) and visible channels. Three visible channels are combined to create composite images of the case studies. Due to a failure in the MAS instrument, the MASTER instrument flew aboard ER-2 as a replacement after 29 July 2007 (Toon et al., 2010); the channels used in this study are common to both instruments.

Supplementary environmental data are required to complete the retrieval. Atmospheric temperature, humidity, and ozone concentration are used to classify the hydrometeor thermodynamic phase and estimate radar and lidar attenuation due to atmospheric gases. These variables are interpolated onto the flight track from the European Centre for Medium-Range Weather Forecasts (ECMWF) Interim Reanalysis (ERA-Interim; Dee et al., 2011).

2.2 Target classification

Prior to the retrieval the contents of each pixel are classified based on a synthesis of radar and lidar measurements. We exploit the instruments' complementary sensitivities to different classes of hydrometeors to infer the presence of liquid cloud, rain and drizzle, and ice. This approach to radar–lidar target classification is similar to that described for CloudSat–CALIPSO in Ceccaldi et al. (2013); however, the categories are simplified in this analysis.

A trade-off in radar and lidar remote sensing is that the hydrometeors with the strongest backscatter also strongly attenuate the beam, weakening its penetration. The sensitivity of lidar to small ice crystals and cloud droplets makes it suited to detecting optically thin ice and liquid cloud, but lidar is therefore quickly attenuated in all but the optically thinnest clouds. In contrast, cloud radar is most sensitive to large hydrometeors, such as ice aggregates and raindrops, and becomes fully attenuated in heavy rain. With the synergy of the two instruments we can use radar to detect optically thick clouds and light to moderate rain, while lidar detects optically thin ice and liquid cloud tops missed by the radar.

The thermodynamic phase of targets is primarily determined by the atmospheric temperature from reanalysis with further distinctions made using thresholds of radar and lidar measurements. At temperatures colder than $-40\,^{\circ}\mathrm{C}$, all targets are classified as ice, and at all temperatures warmer than $0\,^{\circ}\mathrm{C}$ as "warm" liquid cloud or precipitation. Rain and drizzle is inferred at temperatures greater than $0\,^{\circ}\mathrm{C}$ from radar reflectivities greater than $-15\,\mathrm{dBZ}$ (as in Haynes et al., 2011, and others) and may be colocated with warm liquid clouds detected by lidar. In stratiform precipitation we assume that the transition from ice to liquid precipitation occurs in a shallow melting layer (see Sect. 2.3.4); however, in convective precipitation strong attenuation due to heavy rain and melting graupel and hail tends to extinguish the 94 GHz radar. Between -40 and $0\,^{\circ}\mathrm{C}$ the thermodynamic phase of cloud water can be ice, supercooled liquid, or, where the two coexist, mixed phase. First all targets detected by radar are classified as containing ice due to the sensitivity of that instrument to the largest particles. Then liquid and ice as detected by lidar are distinguished based on the vertical gradient of lidar backscatter, which is higher in liquid cloud (Ceccaldi et al., 2013); this method of distinguishing liquid cloud is consistent with the method of Yoshida et al. (2010) using the lidar depolarization ratio. Where radar detects ice and lidar detects liquid, mixed-phase cloud is diagnosed.

The vertical structure and thermodynamic phase of clouds provide constraints on the retrieval of cloud and precipitation properties, but the entire profile is frequently not detectable by both instruments. Therefore the lidar is used to retrieve liquid clouds, but the presence of liquid cloud droplets is an uncertainty in the classification scheme where only radar measurements are available. The lidar is included in the present work for its contribution to the classification of cloud through the vertical profile and for measuring the water content at cloud top; however, the radar is the dominant instrument for the retrieval of rain. As a result of the uncertain presence of liquid clouds within rainy profiles, the radar attenuation that is attributed to rain may be partially due to undiagnosed liquid cloud. Finally, in profiles where the radar is fully attenuated by heavy rain, we assume that rain is continuous to the surface.

2.3 Retrieval methodology

Radar–lidar retrievals of profiles of rain and ice cloud are made using the CAPTIVATE algorithm (cloud, aerosol and precipitation from multiple instruments using a variational technique), an earlier version of which was outlined in Illingworth et al. (2015). In this section we first describe the CAPTIVATE framework and then the main components pertinent to this study: the cost function, the state vector for rain, and the radar forward model. The retrieval is made by iteratively minimizing the cost function to find the state vector that corresponds to the smallest difference between observed and forward-modelled measurements. The state vector consists

of the quantities or parameters of the rain DSD selected as retrieved variables. The forward models are used to estimate the measured variables given the state; the relevant measurements are radar reflectivity factor, PIA, and mean Doppler velocity. In this study we focus on the rain retrieval; details for other hydrometeors will be provided in subsequent papers.

2.3.1 Retrieval framework

The CAPTIVATE algorithm provides a framework for a variational, or optimal estimation, approach to the inverse retrieval (Rodgers, 2000) of vertical profiles of rain, ice and snow, liquid cloud, and aerosols from one or more vertically pointing active and passive instruments. CAPTIVATE is novel in that the measurements used and the state variables retrieved are easily configurable so that the same algorithm can be applied to space-borne, airborne, and ground-based measurements. The retrieved state variables and the representation of each class of hydrometeor can also be modified as appropriate. The variational approach allows for a robust treatment of uncertainties in the retrieval subject to the appropriate selection of observational uncertainties, forward model errors, and physical constraints.

2.3.2 Cost function and minimization

Here we present a general description of the CAPTIVATE retrieval; justifications for the settings used in this study are made in later subsections. The retrieval is made for each profile by iterating to find a state vector that minimizes the cost function given by

$$J = \frac{1}{2}\delta\boldsymbol{y}^{\mathrm{T}}\mathbf{R}^{-1}\delta\boldsymbol{y} + \frac{1}{2}\delta\boldsymbol{x}^{\mathrm{T}}\mathbf{B}^{-1}\delta\boldsymbol{x} + J_{\mathrm{c}}(\boldsymbol{x}), \tag{1}$$

where $\delta\boldsymbol{y} = \boldsymbol{y} - \boldsymbol{y}^{\mathrm{f}}$ is the difference between the observed ($\boldsymbol{y}$) and forward-modelled ($\boldsymbol{y}^{\mathrm{f}}$) measurements; $\mathbf{R}$ is the error covariance matrix of $\delta\boldsymbol{y}$, the sum of the error covariance matrices of the observations and the forward model; $\delta\boldsymbol{x} = \boldsymbol{x} - \boldsymbol{x}^{\mathrm{a}}$ is the difference between the state ($\boldsymbol{x}$) and its a priori estimate ($\boldsymbol{x}^{\mathrm{a}}$); $\mathbf{B}$ is the error covariance matrix of $\boldsymbol{x}^{\mathrm{a}}$ in which the diagonal elements are the error variances of $\boldsymbol{x}$; and $J_{\mathrm{c}}(\boldsymbol{x})$ provides the capability to apply flatness and smoothness constraints to reduce the effect of observational noise on the state vector (Twomey, 1977). Additionally, profiles of retrieved variables can be represented smoothly as a set of cubic spline basis functions (Hogan, 2007, and Sect. 2.3.3). The minimization of the cost function is carried out by iterating on the state vector beginning from the priors in the direction of the first and second derivatives of the cost function (the Levenberg–Marquadt method; Rodgers, 2000).

2.3.3 Rain state variables

The rain DSD is given by a normalized Gamma function of the form

$$N(D) = N_{\mathrm{w}}\frac{\Gamma(4)}{3.67^4}\frac{(3.67+\mu)^{4+\mu}}{\Gamma(4+\mu)}\left(\frac{D}{D_0}\right)^{\mu} \exp\left(\frac{-(3.67+\mu)D}{D_0}\right). \tag{2}$$

This formulation is a function of three independent, physically meaningful parameters for the shape μ, median drop size D_0, and normalized drop number concentration intercept N_{w} of the DSD (Testud et al., 2001; Illingworth and Blackman, 2002). The shape factor μ is of secondary importance to D_0 and N_{w} in terms of the radar reflectivity (Testud et al., 2001) and is poorly constrained by observations (e.g. Moisseev and Chandrasekar, 2007). In this retrieval we use $\mu = 5$, a value derived from both radar and distrometer studies (Wilson et al., 1997; Illingworth and Blackman, 2002). This simplifies the DSD to a two-parameter function of D_0 and N_{w}. The uncertainty due to the assumption of fixed-μ DSD is estimated to be $\pm 15\,\%$ of the rain rate (Wilson et al., 1997), and is included in the uncertainty estimates of the retrieved quantities.

Our primary state variable is the rain rate,

$$R = \frac{\rho_{\mathrm{w}}\pi}{6}\int_0^{\infty} N(D)D^3 v(D)\mathrm{d}D \left[\mathrm{kg\,m^{-2}\,s^{-1}}\right], \tag{3}$$

where ρ_{w} is the density of liquid water, and $v(D)$ is the raindrop terminal velocity as a function of drop size from Beard (1976) corrected for air density through the vertical profile. Hereafter we scale R by a factor of 3600 to express rain rate in units of $\mathrm{mm\,h^{-1}}$. For all retrievals a prior R of $0.1\,\mathrm{mm\,h^{-1}}$ is used. While a prior R is not strictly necessary, it is applied in combination with a large prior variance ($\sigma(\ln R) = 4.0$), such that the retrieved R is relatively insensitive to the prior unless the retrieval is poorly constrained by observations. We note that this value for the prior variance implies that before the measurements are taken we assume there is a 44 % chance of R lying between 0.01 and $1.0\,\mathrm{mm\,h^{-1}}$ and a 56 % chance that R is outside these limits.

The second state variable is N_{w}, so that one state variable is an integral over the DSD, and the second is a parameter of the DSD. Additional state variables increase the degrees of freedom of the retrieval, requiring more information from observational variables as constrains. Therefore we retrieve a single value of N_{w} for each profile with the physical interpretation of representing N_{w} as constant with height or as the vertically averaged value. The representation of N_{w} as constant with height is not expected to be borne out in cases where evaporation or collision–coalescence processes modify the drop number concentration through the vertical profile. We take as the prior N_{w} the number concentration intercept of the Marshall and Palmer (1948) DSD, $8 \times 10^6\,\mathrm{m^{-4}}$.

Table 1. Rain state variables $\boldsymbol{x}_i$ and their prior values $\boldsymbol{x}_i^{\mathrm{a}}$ and uncertainties $\sigma(\boldsymbol{x}_i^{\mathrm{a}})$.

$\boldsymbol{x}_i$	$\boldsymbol{x}_i^{\mathrm{a}}$	$\sigma(\boldsymbol{x}_i^{\mathrm{a}})$	Vertical representation
$\ln R$	$\ln(0.1\,\mathrm{mm\,h^{-1}})$	4.0	Retrieved as the coefficients of a cubic spline basis function with a spacing of 300 m.
$\ln N_{\mathrm{w}}$	$\ln(8\times10^{6}\,\mathrm{m^{-4}})$	3.0	Retrieved as constant with height ($R-N_{\mathrm{w}}$ retrievals) or not retrieved (R-only).
X_{m}	1.0 km	0.0	Not retrieved in this study.

When few observational variables are available, a single-parameter retrieval of R can be made by assuming that N_{w} is constant and equal to its prior, thereby reducing the degrees of freedom so that R is a function of D_0 alone. This is called the R-only retrieval and is similar to CloudSat rain rate retrievals in which N_{w} is assumed constant everywhere. When additional observational variables are available, such as the mean Doppler velocity, there may be sufficient information to also retrieve N_{w}; this is called the $R-N_{\mathrm{w}}$ retrieval.

We use the natural logarithms of R and N_{w} as the state variables with the effect that the values remain positive everywhere and that the algorithm converges in fewer iterations. While in moderate stratiform rain R is often close to invariant with height (e.g. Matrosov, 2007), processes such as evaporation in the lower atmosphere and collision–coalescence in warm clouds will lead to significant variation with height in many contexts. R is therefore represented as the coefficients of a cubic spline basis function with n elements (Hogan, 2007); this has the effect of ensuring that the vertical profile of R is smoothly varying and continuous with height and also of reducing the number of terms in the state vector. Table 1 summarises the rain state variables, their prior values and uncertainties, and their physical representation in each vertical profile. For R-only retrievals the state vector $\boldsymbol{x}$ for a vertical profile is given by

$$\boldsymbol{x} = \ln[R_1 \cdots R_n]^{\mathrm{T}}, \tag{4}$$

while for the $R-N_{\mathrm{w}}$ retrieval the state vector is

$$\boldsymbol{x} = \ln[R_1 \cdots R_n \quad N_{\mathrm{w}}]^{\mathrm{T}}, \tag{5}$$

where N_{w} is assumed constant with height in each profile.

2.3.4 Stratiform precipitation melting layer

We employ a simplified representation of the melting layer in stratiform precipitation by applying radar attenuation between the lowest pixel in each profile classified as ice and the highest pixel classified as rain, provided the two pixels are contiguous. The melting of graupel and hail, usually associated with convective precipitation, are not considered in this melting layer model. Following Matrosov (2008), it is assumed that the two-way attenuation of the melting layer A is proportional to the rain rate R at the first pixel just below the melting layer and the two-way path length X_{m} through the melting layer, such that

$$A = k_{\mathrm{m}} X_{\mathrm{m}} R\ [\mathrm{dB}], \tag{6}$$

where the melting layer extinction coefficient k_{m} is $2.2\,\mathrm{dB\,km^{-1}\,(mm\,h^{-1})^{-1}}$ at 94 GHz and $0.04\,\mathrm{dB\,km^{-1}\,(mm\,h^{-1})^{-1}}$ at 9.6 GHz. The estimated attenuation through the melting layer is based on a Marshall–Palmer DSD for the rain below the melting layer (Matrosov, 2008) and is not modified to match the retrieved DSD in the profile. The thickness of the melting layer and therefore the total attenuation may also depend on the local temperature profile: as sufficient information to retrieve the total melting layer attenuation may be available from the PIA and the attenuation inferred from the radar reflectivity gradient, we include the variable X_{m} in the retrieval to represent the effect of melting layer thickness on radar attenuation; however, in this study X_{m} is held constant with a value of 1.0 km, allowing us to capture the effect of this uncertainty on the retrieved variables and their errors without retrieving X_{m}.

2.3.5 Radar forward model

For a given state vector we estimate the measurements made by each instrument by forward modelling the scattering behaviour between the sensor and each gate for the 94 and 9.6 GHz radars, accounting for the effects of atmospheric gases and hydrometeors.

The radar reflectivity factor of rain is a function of the sixth moment of the DSD,

$$Z = \int_0^\infty N(D) D^6 \gamma_{\mathrm{f}}(D) \mathrm{d}D \left[\mathrm{mm^6\,m^{-3}}\right], \tag{7}$$

where γ_{f} is the Mie–Rayleigh backscatter ratio at the radar frequency f and is required for both 94 and 9.6 GHz radars to account for non-Rayleigh scattering. At 94 GHz the uncertainty of assuming raindrops are spherical Mie scatters is approximately 5 % in integrated backscatter for a gamma DSD with median drop size $D_0 = 1.5$ mm when compared against estimates for oblate spheroids (e.g. Thurai et al., 2007; Zhang et al., 2001) using the **T**-matrix method (Mishchenko et al., 1996).

Scattering and attenuation effects are included in the radar forward model so that the forward-modelled estimate of the apparent radar reflectivity (Z_{a}) is directly comparable to ob-

servations. Attenuation due to atmospheric gases and the dielectric factor of water are calculated from atmospheric temperature and humidity profiles (Liebe, 1985). Multiple scattering effects on radar and lidar backscatter can be estimated within CAPTIVATE using Hogan (2008). Radar reflectivity enhancement due to multiple scattering is especially relevant to space-borne radar measurements at millimetre wavelengths (Battaglia et al., 2005), and the effects on Doppler radar measurements are expected to include both enhanced spectral broadening and modified mean Doppler velocity (Battaglia and Tanelli, 2011); however, with the narrower beam of the airborne radar used in this study we can assume that multiple scattering effects are negligible (Battaglia et al., 2007).

Radar attenuation due to hydrometeors is quantified at each gate by the extinction coefficient

$$k = \frac{\pi}{4} \int_0^\infty Q(D) N(D) D^2 \mathrm{d}D \left[\mathrm{m}^{-1}\right], \tag{8}$$

where $Q(D)$ is the extinction efficiency calculated from Mie theory (Mie, 1908). As for radar reflectivity, the uncertainty in extinction due to assuming spherical drops is less than 2 % for DSD with D_0 of 1.5 mm. The gradient of extinction can be related to the gradient of apparent radar reflectivity and used to estimate the rain rate as suggested by Matrosov (2007). A second approach to quantifying attenuation due to hydrometeors is to measure the two-way path-integrated attenuation,

$$\mathrm{PIA} = 2 \frac{10}{\ln 10} \int_0^\infty k \mathrm{d}z \ [\mathrm{dB}], \tag{9}$$

for each profile. PIA is derived from the radar reflectivity at the ocean surface and included as an observational measurement. Whereas in Matrosov (2007) the gradient method is applied only at moderate to heavy rain rates where it can be assumed that the gradient of apparent radar reflectivity is dominated by attenuation, within the CAPTIVATE scheme both approaches are implemented simultaneously so that the gradient of R and k can be estimated from both the gradient of radar reflectivity and the PIA.

Finally the mean Doppler velocity is the reflectivity-weighted mean drop fall speed,

$$\overline{v}_\mathrm{D} = \frac{-\int_0^\infty N(D) D^6 v(D) \gamma_\mathrm{f}(D) \mathrm{d}D}{\int_0^\infty N(D) D^6 \gamma_\mathrm{f}(D) \mathrm{d}D} \left[\mathrm{m\,s}^{-1}\right], \tag{10}$$

where the terminal fall speed of drops $v(D)$ is from the empirical formulation of Beard (1976) scaled to account for air density changes with altitude and where positive velocities are toward the ground. The forward-modelled mean Doppler velocity is calculated assuming zero vertical air motion; therefore the difference between the forward-modelled and observed mean Doppler velocities will include a contribution from the vertical air motion, which is treated as an observational uncertainty.

Table 2. Observational variables $\boldsymbol{y}_i$ for 94 GHz Doppler radar and their estimated uncertainties $\sigma(\boldsymbol{y}_i)$ as used in the retrieval.

$\boldsymbol{y}_i$	$\sigma(\boldsymbol{y}_i)$	Vertical representation
Z_a	3.0 dB	At each radar gate
$\overline{v}_\mathrm{D}$	1.0 m s^{-1}	At each radar gate
PIA	0.5 dB	Integrated for each profile

The observed variables, their observational uncertainties, and their vertical representation are summarized in Table 2. The uncertainties in the observational variables include both the specified measurement errors for the instrument (Li et al., 2004) and the estimated uncertainties in the radar forward model. We have found that the weighting of errors between radar reflectivity and PIA is quite important for the retrieved rain rate and that if only instrument errors are included the retrieval is not sufficiently constrained by PIA. This is believed to be because attenuation affects all forward-modelled radar reflectivity measurements in the same way, leading to their having strong error correlations. Error correlations are not accounted for in the **R** matrix since they are profile dependent and difficult to estimate, which can lead to the radar reflectivity measurements being overweighted in the retrieval. To overcome this, we take the common approach (e.g. Weston et al., 2014) of inflating the reflectivity errors (and in our case somewhat reducing the errors in PIA) to better balance the information coming from the reflectivity profile and from PIA.

3 Retrievals of rain rate with attenuated radar

The strong attenuation of 94 GHz radar by rain presents a challenge for retrievals of rain rate from profiles of apparent radar reflectivity (Hitschfeld and Bordan, 1954). For nadir-pointing radars, the following ambiguity arises: when the profile of apparent radar reflectivity decreases with range (toward the ground), the decrease could be due either to the attenuation of the radar beam or to a physical change in the rain DSD (e.g. a decrease in R due to evaporation). These two possibilities each constitute a local minimum in the cost function so that a profile of evaporating light rain with negligible attenuation may be wrongly identified as a profile of moderate rain with significant attenuation and visa versa.

To illustrate the double-minimum problem and to visualize how PIA and mean Doppler velocity may help resolve this ambiguity, we use the radar forward model to generate synthetic measurements assuming zero observational noise. In practice, measurement error and more complex profiles

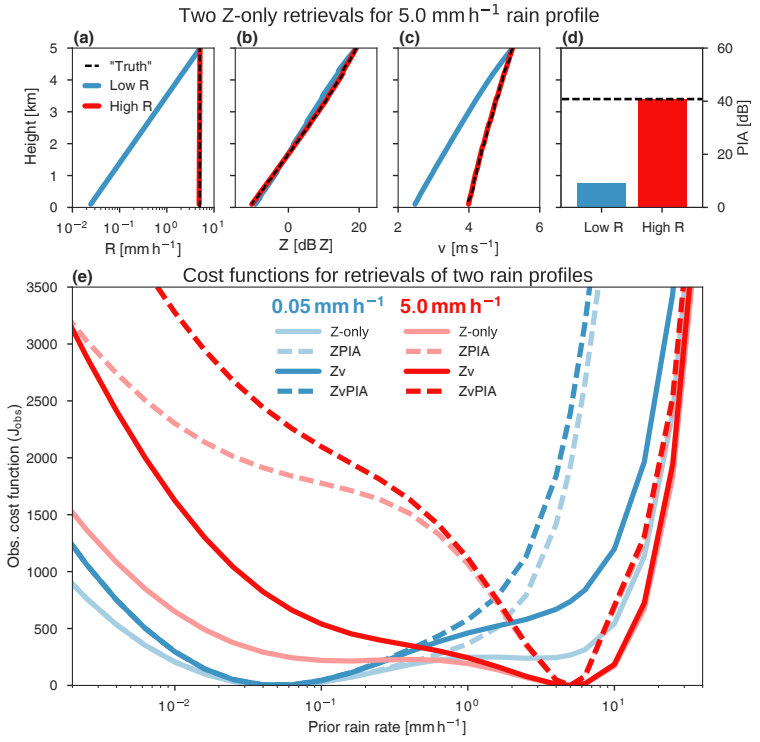

Figure 1. Profiles of **(a)** retrieved rain rate, **(b)** forward-modelled 94 GHz radar reflectivity, **(c)** mean Doppler velocity, and **(d)** PIA for the two solutions to the retrieval from a synthetic profile; dashed lines show the values corresponding to the "true" profile of constant $R = 5.0\,\mathrm{mm\,h^{-1}}$. **(e)** The observational component of the cost function (J_{obs}) for retrievals of two constant rain profiles with $R = 0.05$ and $R = 5.0\,\mathrm{mm\,h^{-1}}$ initialized from a range of R priors. Bimodal or ambiguous retrievals are evident when using radar reflectivity alone (Z-only; light solid lines) and compared against retrievals using additional observational variables (Zv, ZPIA, and ZvPIA; dashed and dark lines) to resolve the ambiguity.

will introduce further uncertainties in the retrieval than in this simplified case. Two profiles of rain are simulated with constant rain rates of 0.0 and $5.0\,\mathrm{mm\,h^{-1}}$ below a level of 5 km and drop number concentration $N_{\mathrm{w}} = 8 \times 6\,\mathrm{m^{-4}}$ to represent a profile of light rain with negligible attenuation and of moderate rain with strong attenuation, respectively. In making the inverse retrieval of the profile of R from a given profile of 94 GHz Z, multiple solutions may be found depending on the prior R: the low-R and high-R profiles of R (Fig. 1a) represent the two minima of the cost function for the retrieval from the radar reflectivity profile (Fig. 1b) corresponding to the $5.0\,\mathrm{mm\,h^{-1}}$ profile of rain (the "truth"). It is evident that the radar reflectivity alone does not provide sufficient information to differentiate between the two solutions; however, the forward-modelled mean Doppler velocity profile (Fig. 1c) and PIA (Fig. 1d) for the two solutions illustrate how additional observational variables may provide sufficient information to resolve the ambiguity. The PIA differs by more than 30 dB between the two solutions and is used effectively to differentiate light and moderate rain in CloudSat rain retrievals. The mean Doppler velocity profiles also differ significantly with the "true" high-R profile varying only slightly with altitude, while the gradient of mean Doppler velocity indicates a reduction in D_0 toward the surface in the low-R profile. An additional advantage of the mean Doppler velocity is that it is not affected by the partial attenuation of the radar.

We can quantify the contribution of the observational variables to resolving ambiguous retrievals by visualizing the cost function. A range of prior rain rates are taken as candidates for the starting point of the retrieval, and for each prior R the contribution of the observations to the cost function is calculated by

$$J_{\mathrm{obs}} = \frac{1}{2} \sum \frac{\left(\boldsymbol{y}^{\mathrm{f}} - \boldsymbol{y}\right)^2}{\sigma_y^2}, \tag{11}$$

which is equivalent to the first term of the cost function in Eq. (1). We can interpret the curve of J_{obs} (Fig. 1e) as showing the tendency of the retrieval algorithm to converge from any prior R toward a local minimum in the cost function, wherein a steeper curve indicates stronger convergence toward a more robust retrieval. To explore the contributions of the observational measurements, we run the retrievals for the two synthetic profiles with only radar reflectivity observations (Z-only), with one additional observational variable (ZPIA, Zv), and with all available observations (ZvPIA).

For the light rain profile, the cost function for the Z-only retrieval has a secondary minimum around 3.0 to 4.0 mm h^{-1}. The bimodal shape of J shows that the retrieval is sensitive to the choice of prior: if R is less than 1.0 mm h^{-1}, the retrieval will converge to the "true" R profile, but if the prior R is greater than 1.0 mm h^{-1} the retrieval will converge on the high-R solution. Conversely, for the moderate rain profile, the Z-only retrieval will converge on a low-R solution if the prior is less than around 0.5 mm h^{-1}. These two solutions are those compared in Fig. 1a–d.

The effect of including PIA (dashed lines in Fig. 1e) is strongest for $R > 1.0$ mm h^{-1}, and this removes any sensitivity to the prior R, while the effect of including Doppler velocity (darker lines in Fig. 1e) is smoother across the full range of R than that of PIA and dominates at low R where radar attenuation is negligible. When both PIA and Doppler measurements are used the effects are cumulative, and the gradient of J shows even stronger convergence toward the unique solution.

This example provides a simple illustration of the bimodal cost function of an R-only rain retrieval with a strongly attenuating 94 GHz radar. Without additional observational measurements, a given profile of radar reflectivity may equally be explained by a strongly attenuating profile with constant R or by a weakly attenuating profile in which R decreases toward the surface. Either PIA or mean Doppler velocity is sufficient to resolve this ambiguity: PIA as a constraint on the total attenuation and mean Doppler velocity on the profile of D_0. As PIA is typically estimated from the ocean surface backscatter, the availability of mean Doppler velocity to resolve these ambiguities presents an opportunity for using Doppler radar to estimate rain rate over land.

4 Retrievals of rain rate and drop number concentration

We now combine PIA and mean Doppler velocity, in addition to radar reflectivity, to make $R - N_w$ rain retrievals from 94 GHz Doppler radar measurements. Three cases of stratiform rain are selected from two ER-2 flights during TC4 (Fig. 2): two flight legs on 22 July 2007 observed rain from melting ice ranging from virga to heavy showers, and a case of light to moderate warm rain from liquid clouds was observed on 29 July 2007.

For each case the $R - N_w$ retrieval is performed using all available measurements from the 94 GHz radar: radar reflectivity, mean Doppler velocity, and PIA. This ZvPIA retrieval is of primary interest for evaluating the full capabilities of the CAPTIVATE retrieval for a Doppler cloud radar; however, we are also interested in the capabilities of a retrieval when one of the observational measurements is not available or has high observational uncertainty. When mean Doppler velocity measurements are not used (ZPIA), the observational variables are analogous to those available to CloudSat over ocean; however, unlike CloudSat rain retrievals, here we retrieve N_w and R. Conversely, when PIA is not used (Zv) the observational variables are similar to those available to a Doppler radar over land where the land surface cannot be sufficiently characterized to estimate PIA. The ZPIA and Zv retrievals of $R - N_w$ are less constrained by observations than the ZvPIA retrieval and will therefore demonstrate some bimodal or poorly constrained retrievals similar to those demonstrated for R-only retrievals in Sect. 3; nevertheless, we include ZPIA and Zv retrievals in order to demonstrate the information provided by the PIA and mean Doppler velocity separately and to identify situations in which a satisfactory $R - N_w$ retrieval may be made with limited observational variables.

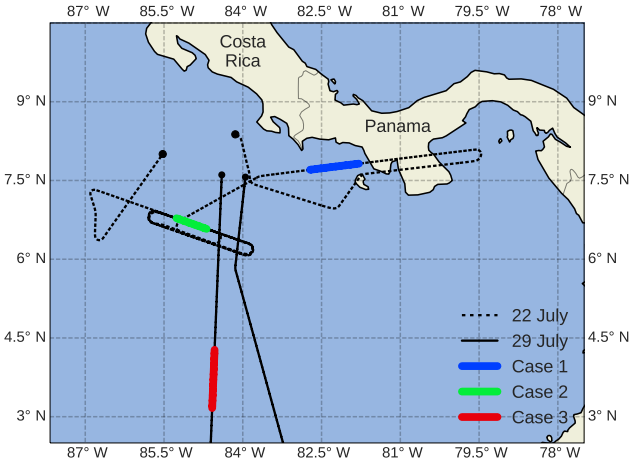

Figure 2. Flight tracks of the NASA ER-2 high-altitude aircraft over the tropical eastern Pacific on 22 and 29 July 2007 during the TC4 field campaign. The flight legs selected for case studies of stratiform rain are highlighted.

In each case the retrieval is evaluated by forward modelling all 94 and 9.6 GHz radar variables, whether or not they were assimilated in the retrieval, and comparing against the observations.

4.1 Case 1: moderate rain from melting ice, 22 July 2007

Stratiform rain from melting ice provides a test of many of the simplifying assumptions made in rain retrievals. At moderate and heavy rain rates we expect R to be close to constant with height unless significant evaporation is evident (Haynes et al., 2009). N_w may be expected to be close to values deemed typical by Marshall and Palmer (1948) or Testud et al. (2001), i.e. between 2.0×10^6 and 8.0×10^6 m^{-4} and constant with height (Tokay and Short, 1996). From in situ measurements of stratiform rain we expect median drop sizes to be in the range 1.0–1.5 mm (Tokay and Short, 1996).

Between 15:54 and 16:03 UTC on 22 July 2007, ER-2 overflew approximately 110 km of precipitating stratiform

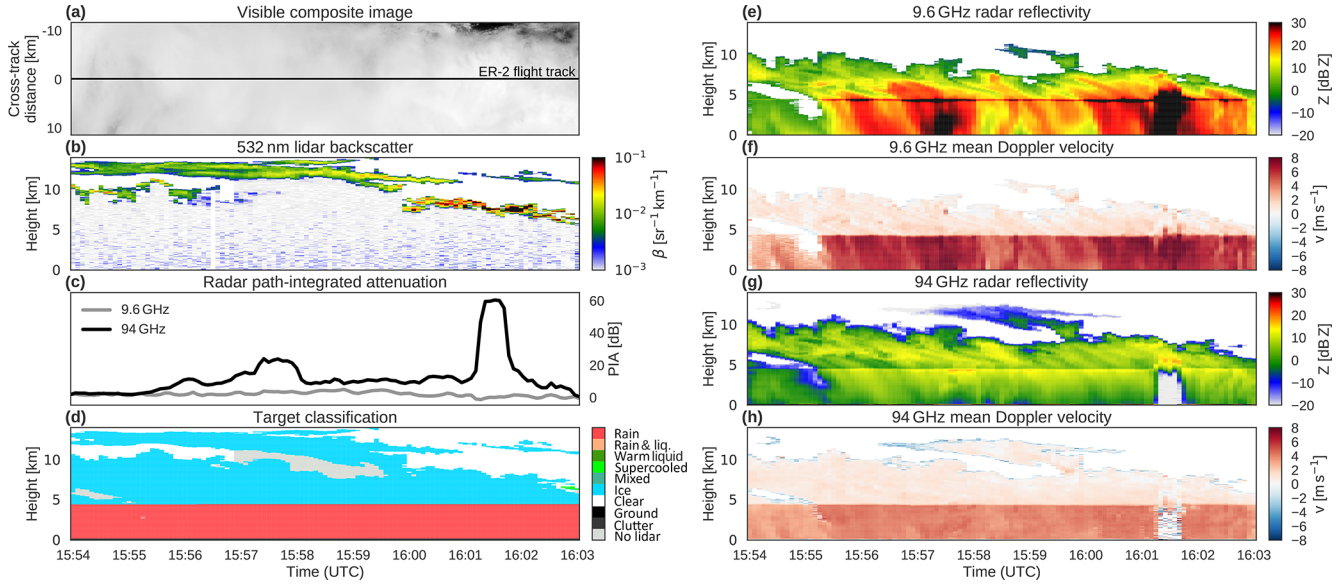

Figure 3. Selected measurements made by ER-2 instruments for Case 1 between 15:54 and 16:03 UTC on 22 July 2007 as part of TC4. Composite cloud scene **(a)** from MAS/MASTER visible channels with the ER-2 flight track marked; 532 nm lidar backscatter **(b)**; 9.6 and 94 GHz radar PIA **(c)**; target classification from radar–lidar synergy **(d)**; 9.6 GHz radar reflectivity **(e)** and mean Doppler velocity **(f)**; and 94 GHz radar reflectivity **(g)** and mean Doppler velocity **(h)**.

cloud around 50 km south of the coast of Panama (Fig. 2). Radar, lidar, and radiometer measurements (Fig. 3) reveal distinct regimes of light, moderate, and heavy rain below a melting layer at around 4.5 km a.s.l. (above sea level), contiguous with ice clouds with tops between 6 and 10 km. The scene is overlain by cirrus between 10 and 15 km, which is primarily detected by the lidar. In light rain between 15:54 and 15:55 UTC, the 94 GHz radar is barely attenuated. Moderate stratiform rain follows from 15:55 and 16:03 UTC with a strong 9.6 GHz bright band evident and 94 GHz PIA between 5 and 50 dB. Finally a heavy shower is embedded within the moderate rain between 16:01 and 16:02 UTC. In the latter regime the 94 GHz radar is completely attenuated such that PIA saturates around 60 dB; 94 GHz radar reflectivity and mean Doppler velocity measurements are therefore not available within these heaviest rain profiles.

The retrieved variables (Fig. 4a–e) and forward-modelled 94 and 9.6 GHz radar measurements (Fig. 4f–j) are compared for the ZvPIA, Zv, and ZPIA retrievals. We evaluate the retrievals at a height of 3 km a.s.l. approximately 1 km below the melting layer.

4.1.1 Moderate rain (15:55–16:01 and 16:02–16:03 UTC)

In the moderate rain regime the ZvPIA retrieval estimates rain rates of 1.0–2.0 mm h^{-1} at the melting layer. In profiles with strong attenuation (PIA up to 20 dB), R is close to constant from the melting layer to the surface; conversely, in less attenuated profiles (with PIA around 10 dB) some evaporation is evident with R reducing to 0.1–1.0 mm h^{-1} at the surface (Fig. 4a). Estimates of N_w are consistently between 10^6 and 10^7 m^{-4} in this regime (Fig. 4c), close to the Marshall and Palmer (1948) value, while D_0 is around 1.0 mm at the melting layer and decreases somewhat toward the surface in profiles where evaporation is strong (Fig. 4d). Forward-modelled 94 GHz radar measurements agree with observations at 3 km (Fig. 4f–h), as expected since the retrieval minimizes differences between the observed and forward-modelled variables. The 9.6 GHz radar measurements forward-modelled from the retrieved state show generally good agreement with independent observations at 3 km a.s.l. (Fig. 4i and j), although 9.6 GHz radar reflectivity is overestimated by as much as 3 dB in profiles with strong evaporation between 15:58 and 16:00 UTC, and mean Doppler velocity is underestimated in the profiles with the heaviest rain.

The averaged vertical profiles of the ZvPIA retrieval in moderate rain (Fig. 5) show that the forward-modelled 94 GHz radar reflectivity is overestimated near the surface, while the largest error in 9.6 GHz is in the mean Doppler velocity in the lowest 2–3 km. We suggest that these errors in the forward-modelled variables through the vertical profile relate to the representation of N_w as constant with height such that the effects of evaporation on the DSD – a decrease in concentration of the smallest drops – is not resolved. The ZvPIA retrieval is broadly able to reproduce the 9.6 GHz radar reflectivity while slightly underestimating mean Doppler velocity.

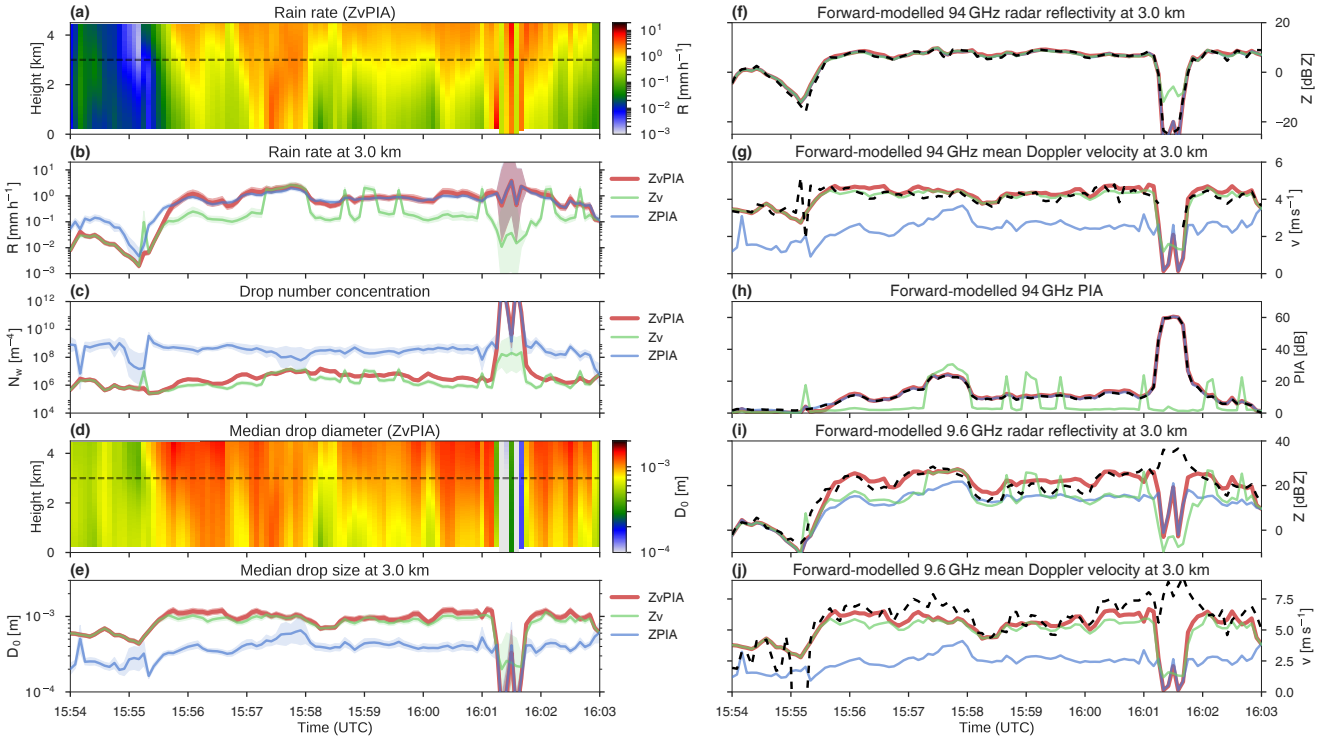

Figure 4. Time series of 94 GHz ZPIA, Zv, and ZvPIA retrievals compared for Case 1 between 15:54 and 16:13 UTC on 22 July 2007. Retrieved state and derived variables **(a–e)** and forward-modelled radar measurements **(f–j)** for the three retrievals are shown at a height of 3 km a.s.l. (above sea level; indicated with a light dashed line in the left-hand scenes), while the full scenes of R **(a)** and D_0 **(d)** are shown for the ZvPIA retrieval. Shading indicates the 1σ uncertainty in the retrieved and derived variables. Dark dashed lines (right) indicate the observed radar measurements.

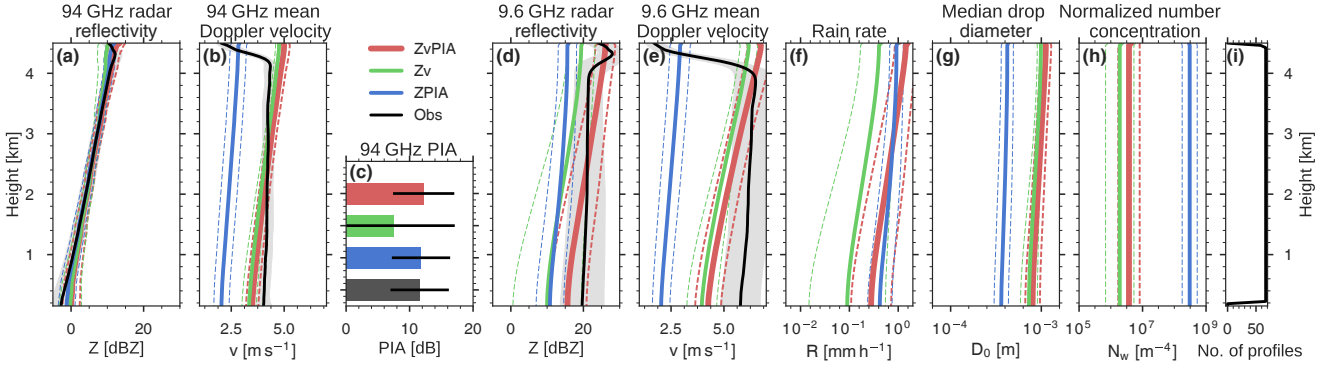

Figure 5. Averaged profiles of moderate rain between 15:55:30 and 16:11:00 UTC on 22 July 2007. Forward-modelled 94 GHz radar reflectivity **(a)**, mean Doppler velocity **(b)**, and PIA **(c)**; forward-modelled 9.6 GHz radar reflectivity **(d)** and mean Doppler velocity **(e)**; and retrieved rain rate **(f)**, median drop size **(g)**, and number concentration parameter **(h)** for ZPIA, Zv, and ZvPIA retrievals. The number of profiles included at each height is indicated in **(i)**. Shading and dashed lines indicate the 1σ uncertainty in the retrieved and derived variables.

The ZPIA and Zv retrievals illustrate the contributions of mean Doppler velocity and PIA to a ZvPIA retrieval and the ambiguities that arise in under-constrained retrievals. Both ZPIA and Zv retrievals are considerably more sensitive to the selection of priors and prior uncertainties than the ZvPIA retrieval. At 3 km a.s.l. (Fig. 4), ZPIA estimates of R in the moderate rain regime are close to those of ZvPIA, but N_w and D_0 differ significantly with ZPIA estimating a much higher concentration of smaller drops than ZvPIA. The forward-modelled mean Doppler velocity shows that this retrieval leads to large errors in drop fall speeds. Conversely, the Zv retrieval tends to underestimate rain rate in this regime by

up to an order of magnitude, tending toward the prior R of 0.1 mm h^{-1} except in the strongly attenuated profiles between 15:57 and 15:58 UTC where Zv is, perhaps surprisingly, able to reproduce the observed PIA from the profiles of radar reflectivity and mean Doppler velocity. While D_0 is well constrained by the mean Doppler velocity, without a constraint on PIA the forward-modelled observations confirm that the Zv retrieval tends to represent weakly attenuating profiles of rain; the forward-modelled 9.6 GHz variables show that this retrieval leads to a significantly underestimated radar reflectivity.

4.1.2 Light rain (15:54–15:55 UTC)

In the light rain regime, ZvPIA estimates R in the range 0.002–0.1 mm h^{-1} and N_w in the range 10^5–10^6 m^{-4}. The lower rain rate corresponds to an observed 1.0 m s^{-1} decrease in 94 GHz mean Doppler velocity compared to the moderate rain regime; the retrieval resolves smaller drops in the light rain with D_0 around 0.5 mm. The forward-modelled 9.6 GHz radar measurements from the ZvPIA retrieval are consistent with independent observations.

Zv retrieves R consistent with ZvPIA throughout the light rain regime, while ZPIA somewhat overestimates R in these profiles. PIA is negligible and provides little additional information in this regime; therefore the ZPIA retrieval represents a higher concentration of smaller drops as the retrieved R and N_w tend toward the priors. This sensitivity to the prior when observational information is limited was demonstrated in Sect. 3, and as in that synthetic case, the ZPIA retrieval here could be improved with a more appropriate prior. In contrast, with mean Doppler velocity as a constraint on drop size the DSD retrieved by Zv is very close to that of ZvPIA. The strong performance of Zv in light rain suggests potential for using Doppler radar for $R - N_w$ retrievals of light rain over land.

4.1.3 Heavy shower (16:01–16:02 UTC)

The upper limit of the 94 GHz radar frequency for rain retrievals is reached in the heavy shower where PIA is saturated and no radar reflectivity or mean Doppler velocity is available below the melting layer. With limited observational constraints, both ZvPIA and ZPIA retrievals estimate R between 0.5 and 5.0 mm h^{-1}; large uncertainties in R reflect the dearth of information available. The errors in forward-modelled 9.6 GHz radar measurements at 3 km suggest that the true rain rate lies on the upper end of this uncertainty range at around 10 mm h^{-1}; this is confirmed by a retrieval assimilating both 94 and 9.6 GHz radar variables in Sect. 5. Without PIA information, the Zv retrieval interprets the deficit in radar reflectivity as a drop in rain rate and drop size, adding uncertainty to the retrieved quantities. The estimates of N_w vary over many orders of magnitude and are clearly unconstrained by observations in this regime, demonstrating that the $R - N_w$ retrieval is not warranted without sufficient observational information. The PIA continues to provide a constraint on rain rate but becomes saturated once the radar is fully attenuated.

In this case of tropical stratiform rain the 94 GHz radar is fully attenuated by rain rates up to 10 mm h^{-1} falling from a melting layer at around 4.0 km a.s.l. In the midlatitudes, however, where melting layers are much shallower, successful $R - N_w$ retrievals should be possible up to higher rain rates before the radar is fully attenuated.

4.1.4 Joint frequencies of retrieved and forward-modelled variables

A more comprehensive evaluation of the retrievals against independent 9.6 GHz radar measurements can be made using the joint frequencies of retrieved state variables (Fig. 6a–6c) and forward-modelled 9.6 GHz radar measurements (Fig. 6d–f) for each retrieval. The major modes in the rain retrieval are evident in the distributions of R and N_w relative to the priors (dashed lines) and in the distribution of forward-modelled 9.6 GHz radar reflectivity and mean Doppler velocity compared against observations (black contours). In the 9.6 GHz radar variables the moderate rain regime exhibits radar reflectivity between 20 and 30 dB Z and mean Doppler velocity between 6 and 7 m s^{-1}, while the light rain regime has radar reflectivity between 0 and 5 dB Z and a mean Doppler velocity of around 3 m s^{-1}.

The ZPIA retrieval has a dominant mode corresponding to the moderate rain regime with R between 0.5 and 2.0 mm h^{-1} and a higher N_w with respect to the prior; without mean Doppler velocity this retrieval represents a relatively high concentration of small drops. The corresponding forward-modelled measurements shows that the small drop size leads to a significant underestimation of both mean Doppler velocity and radar reflectivity at 9.6 GHz.

Without PIA, Zv retrievals in the moderate rain regime tend toward weakly attenuated profiles with N_w less than 10^6 m^{-4}, where R is close to the prior. This leads to underestimates of radar reflectivity by more than 10 dB; the mean Doppler velocity is reasonably well constrained but broadly underestimated by around 1 m s^{-1}. A secondary mode with N_w close to the prior and R greater than 1 mm h^{-1} represents the strongly attenuated profiles of moderate rain in which Zv comes close to reproducing the observed PIA. Light rain profiles are represented with $N_w \approx 10^6$ m^{-4}, somewhat overestimating mean Doppler velocity.

ZvPIA resolves distinct modes for light and moderate rain regimes in the retrieved variables, and each mode corresponds well to the observed 9.6 GHz radar measurements: the moderate rain regime is represented with heavier rain than the Zv retrieval but with a lower concentration of smaller drops than the ZPIA retrieval; the light rain regime is similar to that of the Zv retrieval where the negligible PIA provides little additional information. Both rain regimes

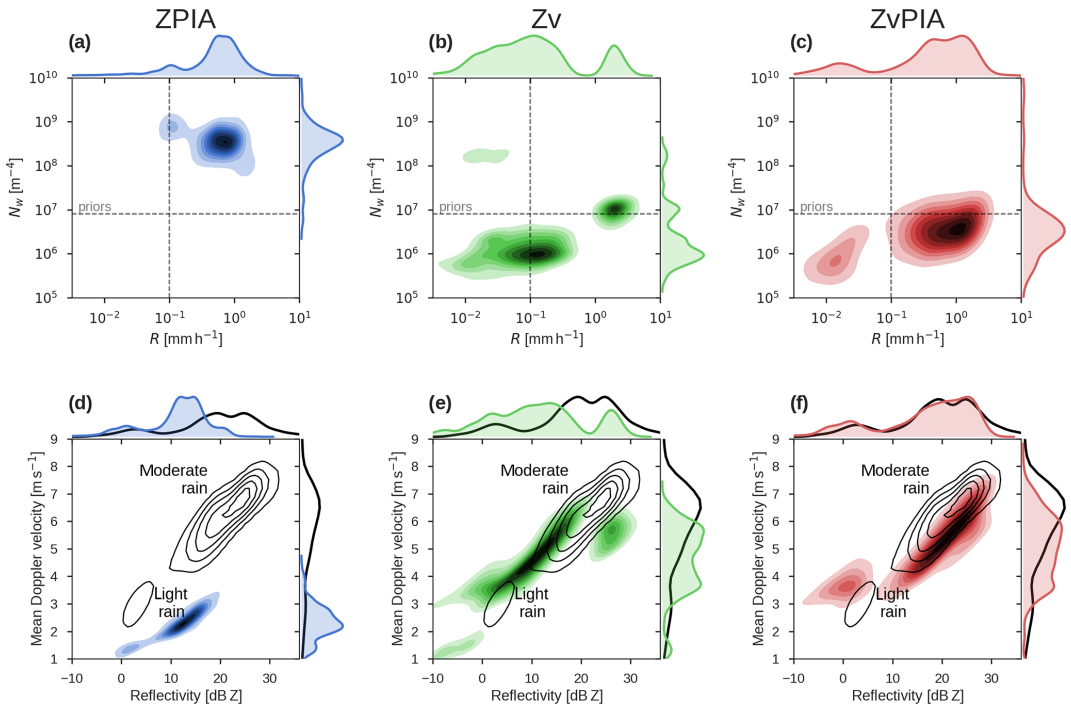

Figure 6. Joint (filled contours) and univariate (curves) kernel density estimation histograms of retrieved rain state variables R and N_w **(a–c)** and forward-modelled EDOP measurements **(d–f)** for ZPIA **(a, d)**, Zv **(b, e)**, and ZvPIA **(c, f)** rain retrievals during Case 1 on 22 July 2007. Dashed lines indicate the values of the prior state variables used in the retrieval. Black contours indicate the distribution of independent EDOP measurements; the major rain regimes are labelled.

have N_w between 10^6 and 10^7 m^{-4}, which is consistent with the average value of 2×10^6 m^{-4} for stratiform rain found by Testud et al. (2001). The 9.6 GHz radar reflectivity is well represented across both rain regimes; however, the mean Doppler velocity shows that drop fall speed is slightly underestimated in moderate rain and overestimated in the light rain; this may be due to representing N_w as constant with height in each profile such that any variations in the DSD with height are expressed as changes in drop size rather than in drop number concentration.

We have retrieved R as a function of both D_0 and N_w for a case of stratiform rain from melting ice, including rain rates from light rain as low as 10^{-3} mm h^{-1}, to moderate rain with R up to 10 mm h^{-1}. The retrieved N_w was around 10^6 m^{-4} throughout the case, which is consistent with expectations for average drop number concentrations in this context; the exception is in the heavy rain shower where the 94 GHz radar becomes fully attenuated, and insufficient information is available for $R - N_w$ retrieval. The Zv retrieval, an analogue for Doppler radar retrievals over land, performed very well in light rain where PIA is close to zero but tended towards the priors in moderate rain. ZPIA retrievals without mean Doppler velocity tend to estimate R broadly accurately but retrieve DSDs with a high concentration of small drops, leading to errors with respect to the independent radar measurements; indeed, since the estimated N_w values were close to expectations in this context, a good non-Doppler retrieval of R could have been made by assuming that the value of N_w is equal to the prior.

4.2 Case 2: evaporating rain from melting ice, 22 July 2007

We now evaluate the $R - N_w$ retrieval for a case of very light rain from melting ice, much of which evaporates before reaching the ground. ER-2 overflew a 60 km section of stratiform cloud 300 km south of Costa Rica between 13:12 and 13:17 UTC on 22 July 2007. Light rain was observed below clouds with tops between 10 and 12 km (Fig. 7). Below the melting layer, both 94 and 9.6 GHz radar reflectivities are less than 10 dB Z and decrease toward the surface; the exception is a region of higher 9.6 GHz radar reflectivity between 13:16 and 13:17 UTC where 94 GHz PIA is small but nonzero at around 3 dB Z. In combination with the low 94 GHz PIA, the observations suggest significant evaporation in the lower atmosphere, including virga.

Time series of retrieved variables (Fig. 8a and e) and forward-modelled 94 and 9.6 GHz radar measurements (Fig. 8f and j) are evaluated against observations. We compare ZPIA, Zv, and ZvPIA retrievals at a height of 4 km a.s.l., which is just below the melting layer.

ZvPIA makes a consistent representation of evaporating light stratiform rain with R between 0.1 and 0.2 mm h^{-1}

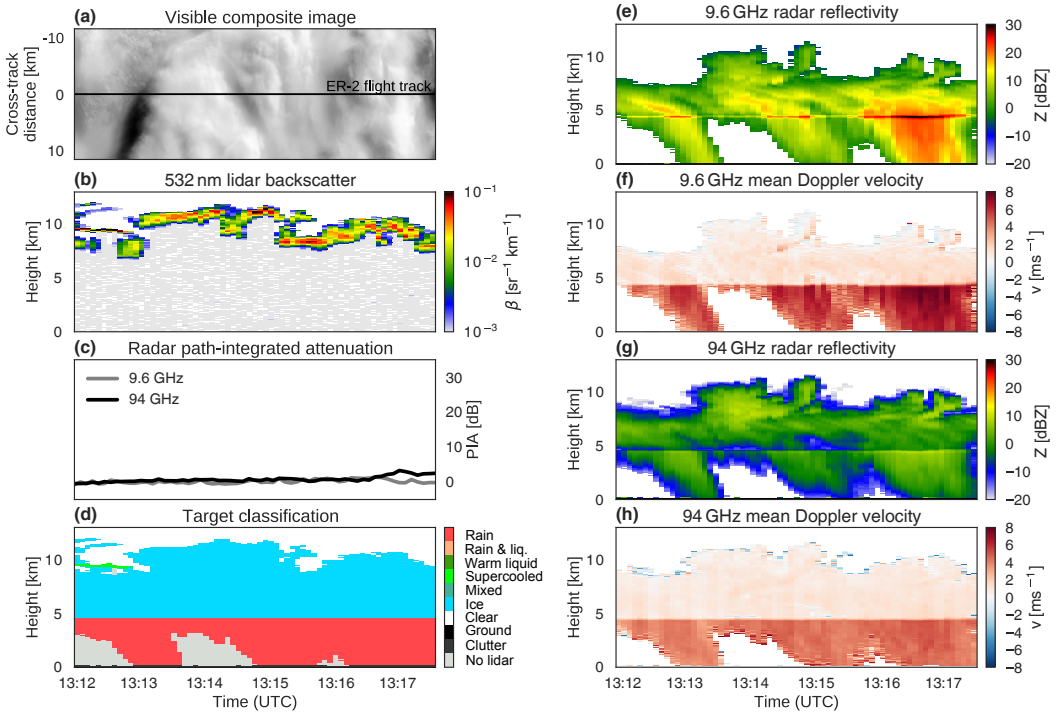

Figure 7. Selected measurements made by ER-2 instruments for Case 2 between 13:12:00 and 13:17:30 UTC on 22 July 2007 as part of TC4. The composite cloud image from MAS/MASTER visible channels **(a)** with the ER-2 flight track marked; 532 nm lidar backscatter **(b)**; 9.6 and 94 GHz radar PIA **(c)**; target classification from radar–lidar synergy **(d)**; 9.6 GHz radar reflectivity **(e)** and mean Doppler velocity **(f)**; and 94 GHz radar reflectivity **(g)** and mean Doppler velocity **(h)**.

at the melting layer down to a minimum detectable rate of 10^{-3} mm h^{-1} or at the limits of the virga. In the heaviest rain profiles between 13:16 and 13:17 UTC, R is around 0.1 mm h^{-1} at the surface with D_0 as large as 1.5 mm. Retrieved N_w is consistently around 10^5 m^{-4}, an order of magnitude lower than the previous case of stratiform rain from melting ice and significantly lower than the prior. Forward-modelled 9.6 GHz radar variables show good agreement with independent measurements at 4 km a.s.l.; however, the averaged vertical profiles (Fig. 9) show that, while the vertical profile of 94 GHz variables are well represented, 9.6 GHz radar reflectivity is strongly underestimated in the lowest 3 km. We suggest that these errors in the vertical distribution are due to the effects of evaporation on the DSD, which are not fully resolved when N_w is constant with height. We would expect N_w to decrease toward the surface as the smallest drops evaporate, while underestimates in the forward-modelled mean Doppler velocity at both radar frequencies suggest that the median raindrop size may be too small near the surface.

Similar to the light rain profiles of Case 1, both ZPIA and Zv retrievals make estimates of R close to the ZvPIA retrieval. ZPIA retrievals slightly overestimate R with N_w 2 to 3 orders of magnitude higher than ZvPIA estimates; the corresponding low D_0 of around 0.5 mm leads to significant errors in mean Doppler velocity. In contrast, Zv estimates of D_0 are well constrained by mean Doppler velocity, and where PIA is negligible the Zv retrieval is identical to that of ZvPIA. As noted in the previous case, this indicates that it may be possible to make $R - N_w$ retrievals of light rain over land with Doppler radar.

4.3 Case 3: warm rain from liquid clouds, 29 July 2007

In warm rain from liquid clouds, we expect a distinct DSD with a higher concentration of smaller drops and drop growth between cloud top and the surface (Lebsock et al., 2011). On 29 July 2007, ER-2 overflew a 120 km section of precipitating warm marine cloud around 500 km south of Costa Rica between 12:41 and 12:51 UTC (Fig. 10). In the first part of the flight (12:41–12:46 UTC) observations suggest moderate rainfall with deeper cloud tops around 3.5 km: PIA varies between 10 and 50 dB in narrow features where 9.6 GHz radar reflectivity exceeds 20 dB Z. The following section (12:46–12:51 UTC) is characterized by shallower stratiform cloud with tops around 3 km and is associated with patchy light precipitation and PIA between 0 and 10 dB.

Concurrent to the rain retrieval shown here, we use the lidar to retrieve liquid cloud, which also contributes to the attenuation of 94 GHz radar. The retrieved properties of the liquid cloud do not vary between the different retrievals com-

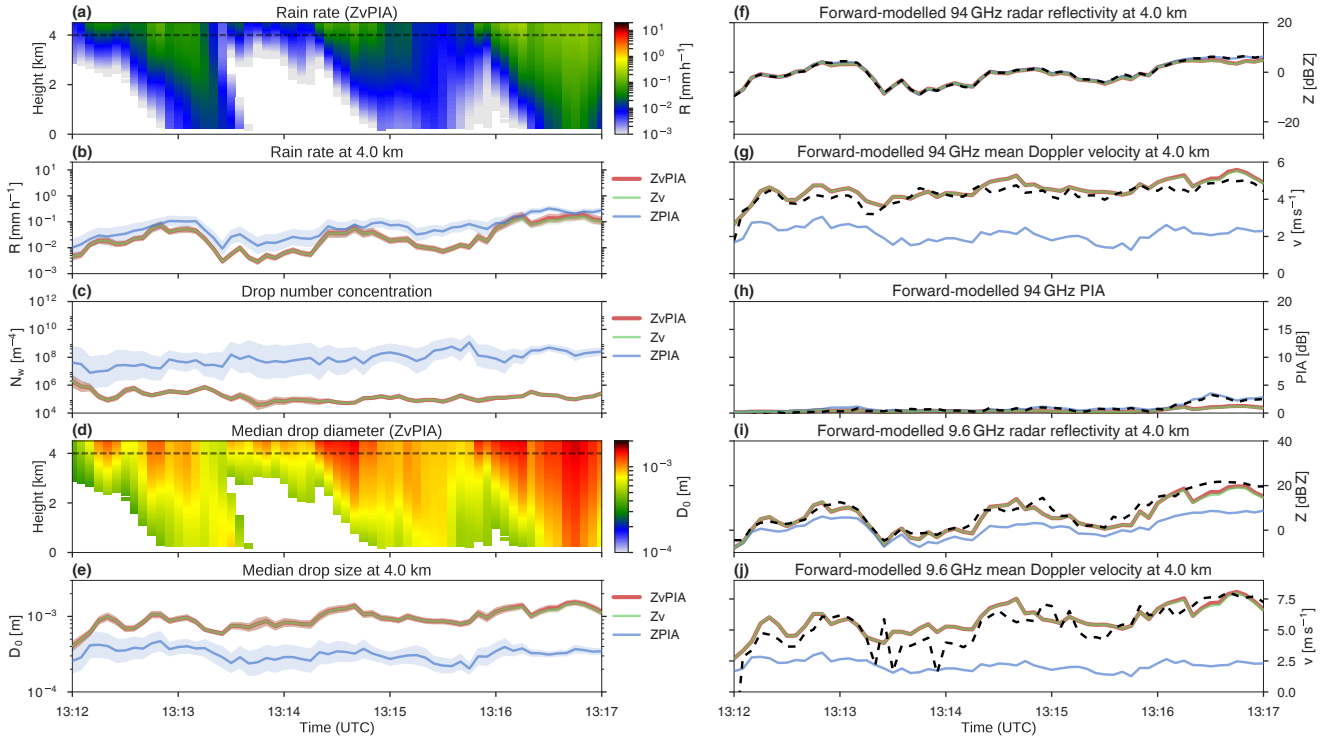

Figure 8. Time series of 94 GHz ZPIA, Zv, and ZvPIA retrievals compared for Case 2 between 13:12 and 13:17 UTC on 22 July 2007. Retrieved state and derived variables **(a–e)** and forward-modelled radar measurements **(f–j)** for the three retrievals are shown at a height of 4 km a.s.l. (indicated with a dashed line in the left-hand scenes), while the full scenes of R **(a)** and D_0 **(d)** are shown for the ZvPIA retrieval. In this case the observed PIA is negligible, so the ZvPIA retrieval has no more information than the Zv retrieval and the two lines are overlaid. Shading indicates the 1σ uncertainty in the retrieved and derived variables. Black dashed lines indicate the observed radar measurements for comparison with the retrievals.

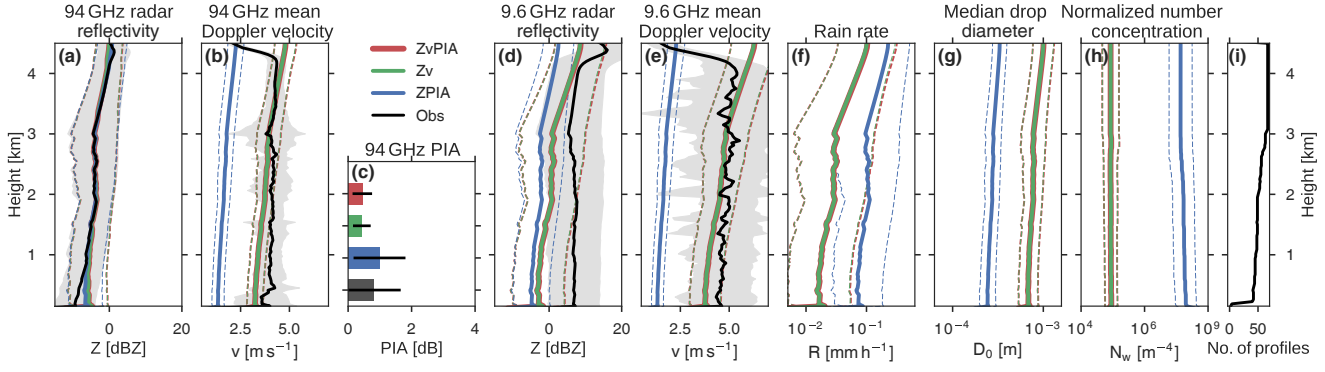

Figure 9. Averaged profiles of evaporating light rain between 13:12 and 13:17 UTC on 22 July 2007. Forward-modelled 94 GHz radar reflectivity **(a)**, mean Doppler velocity **(b)**, and PIA **(c)**; forward-modelled 9.6 GHz radar reflectivity **(d)** and mean Doppler velocity **(e)**; and retrieved rain rate **(f)**, median drop size **(g)**, and number concentration parameter **(h)** for ZPIA, Zv, and ZvPIA retrievals. The number of profiles included at each height is indicated in **(i)**. Shading and dashed lines indicate the 1σ standard deviation of the retrieved and derived variables.

pared here, and we do not evaluate the retrieval of cloud liquid water content in this study; however, as discussed in Sect. 2.2, lidar is quickly extinguished at cloud top and radar is most sensitive to drizzle drops, so cloud base is rarely known in the target classification. Hence we acknowledge that the simultaneous retrieval of cloud and precipitation in warm clouds from 94 GHz radar is a source of uncertainty that warrants further consideration (e.g. Haynes et al., 2009; Hawkness-Smith, 2010; Mace et al., 2016).

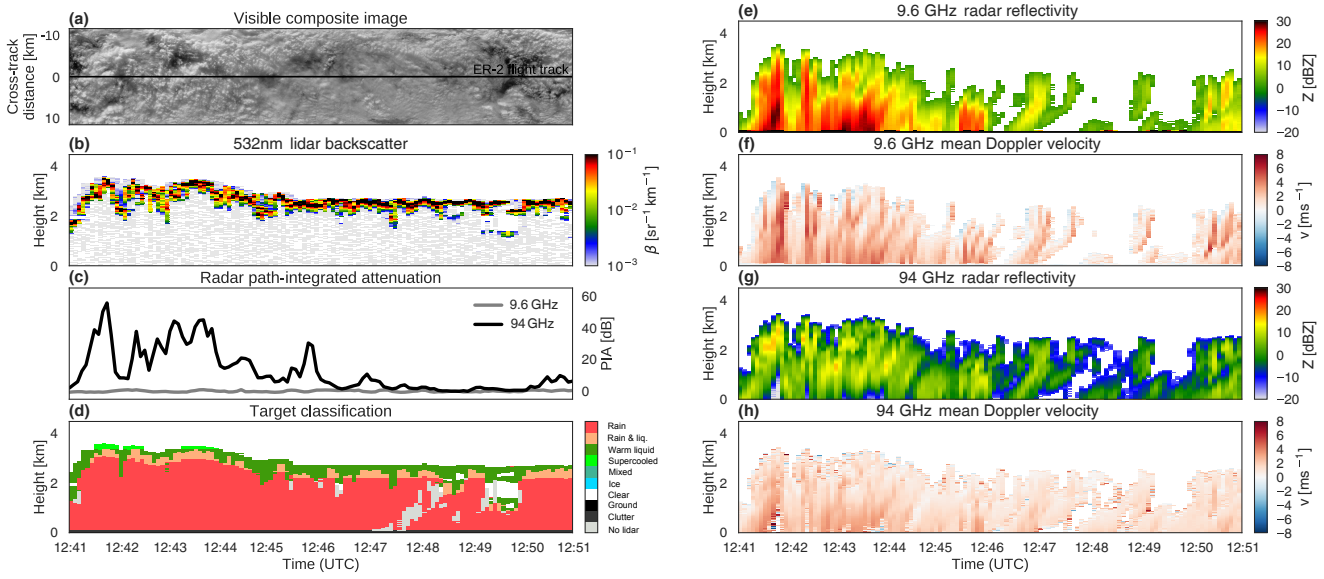

Figure 10. Selected measurements made by ER-2 instruments for Case 3 between 12:41 and 12:51 UTC on 29 July 2007 as part of TC4. Composite cloud scene **(a)** from MAS/MASTER visible channels with the ER-2 flight track marked; 532 nm lidar backscatter **(b)**; 9.6 and 94 GHz radar PIA **(c)**; target classification from radar–lidar synergy **(d)**; 9.6 GHz radar reflectivity **(e)** and mean Doppler velocity **(f)**; and 94 GHz radar reflectivity **(g)** and mean Doppler velocity **(h)**.

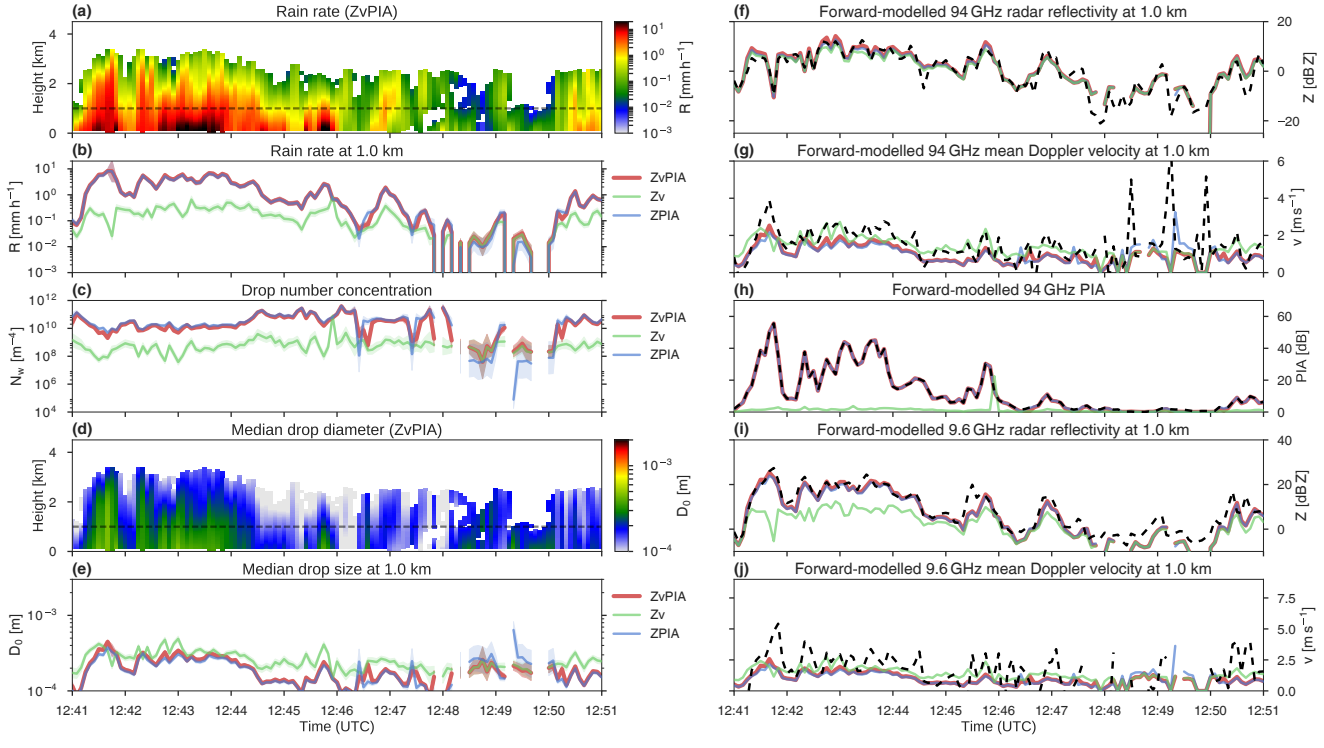

Figure 11. Time series of ZPIA, Zv, and ZvPIA 94 GHz retrievals for Case 3 on 29 July 2007. Retrieved state and derived variables **(a–e)** and forward-modelled radar measurements **(f–j)** for the three retrievals are shown at a height of 1 km a.s.l. (indicated with a light dashed line in the left-hand scenes), while full scenes of R **(a)** and D_0 **(d)** are shown for the ZvPIA retrieval. Shading indicates the 1σ uncertainty in the retrieved and derived variables. Dark dashed lines **(f–j)** indicate the observed radar measurements.

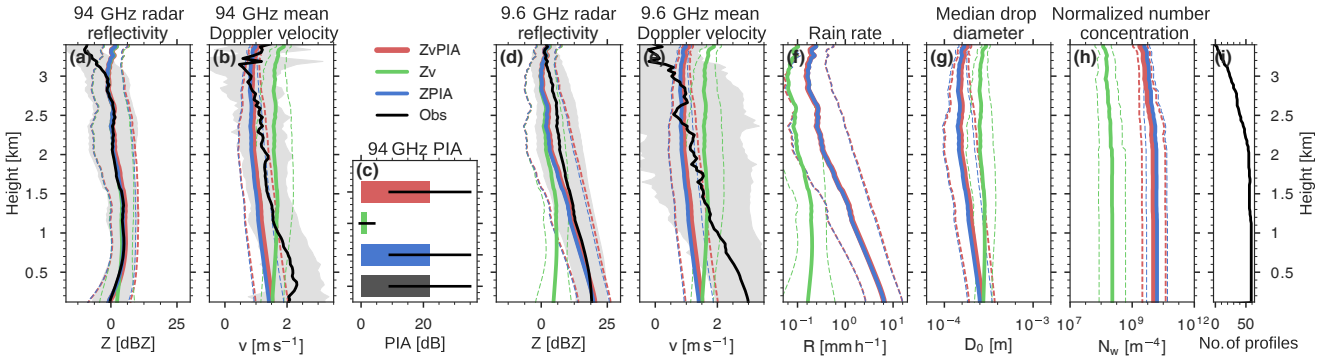

Figure 12. Averaged profiles of moderate rain between 12:41 and 12:46 UTC on 29 July 2007. Forward-modelled 94 GHz radar reflectivity **(a)**, mean Doppler velocity **(b)**, and PIA **(c)**; forward-modelled 9.6 GHz radar reflectivity **(d)** and mean Doppler velocity **(e)**; and retrieved rain rate **(f)**, median drop size **(g)**, and number concentration parameter **(h)** for ZPIA, Zv, and ZvPIA retrievals. The number of profiles included at each height is indicated in **(i)**. Shading and dashed lines indicates the 1σ standard deviation of the retrieved and derived variables.

The retrieved variables (Fig.11a–e) and forward-modelled radar measurements (Fig.11f–j) are compared at 1 km a.s.l. and compared against 94 and 9.6 GHz radar measurements. We compare ZPIA, Zv, and ZvPIA retrievals as in the previous cases. Warm rain or drizzle forming in liquid clouds can be easily distinguished from rain falling below ice clouds within the target classification scheme so that physically appropriate choices for the priors and the physical representations of state variables can be configured in CAPTIVATE for distinct warm and "cold" rain regimes; however, in this study we use the same prior R and N_w throughout.

4.3.1 Moderate rain (12:41–12:46 UTC)

The ZvPIA retrieval resolves a strong increase in rain rate from cloud top, where R is between 0.1 and 1.0 mm h^{-1}, to the surface, where R increases to 1.0–10.0 mm h^{-1}. Retrieved N_w is consistently around 10^{10} m^{-4} in the moderate rain regime, several orders of magnitude greater than estimated for rain from melting ice; accordingly, the drops are much smaller with D_0 increasing from 0.1–0.3 mm at cloud top to 0.2–0.5 mm near the surface. At 1 km a.s.l. the 94 GHz radar measurements correspond very well to the forward-modelled variables. The 9.6 GHz radar reflectivity is also close to the forward model; however, while the forward-modelled mean Doppler velocity at 9.6 GHz also tracks well with observations, peaks associated with the heaviest precipitation features are not resolved.

The vertical structure of 94 and 9.6 GHz radar reflectivity is well represented in the ZvPIA retrieval over the moderate warm rain regime (Fig. 12); however, mean Doppler velocity is underestimated by around 1 m s^{-1} in the lowest 1 km at both radar frequencies. The retrieval of constant N_w for each profile allows for a broadly satisfactory retrieval of the rain DSD with a good fit to observations, but the full vertical profiles show that some microphysical processes are not resolved: in warm rain we expect collision and coalescence to lead to both an increase in drop size and a decrease in drop number concentration toward the surface. It seems likely, as for the representation of evaporation in case 2, that while the retrieval of N_w allows for an improved retrieval of the DSD across a range of rain regimes, there are limits to the vertical variability in the DSD that can be resolved with a height-invariant N_w.

The ZPIA retrieval closely resembles ZvPIA; this includes matching estimates of D_0 despite having no constraint on drop size from mean Doppler velocity. Zv retrieves similar D_0 but underestimates N_w by as much as 2 orders of magnitude: the Zv-retrieved DSD has fewer drops and negligible PIA at 94 GHz, which corresponds to very large errors in forward-modelled 9.6 GHz radar reflectivity. Unlike the stratiform rain cases, here PIA is more important for an accurate retrieval than mean Doppler velocity: the mean Doppler velocity may be less sensitive to the changes in the terminal fall speed of small drops, while PIA in combination with radar reflectivity provides an effective constraint on the number concentration because only a DSD with many small drops satisfies the observed strong attenuation and low radar reflectivity.

4.3.2 Light rain (12:46–12:51 UTC)

In the light warm rain, ZvPIA estimates patchy precipitation features with R between 0.01 and 0.5 mm h^{-1} and D_0 around 0.1–0.3 mm, similar to values at the tops of the deeper warm clouds but without significant drop growth toward the surface. The retrieved N_w in the lightest rain profiles is around 10^8–10^9 m^{-4} but returns to 10^{10} m^{-4} where heavier rain features are evident. The forward-modelled radar reflectivities are close to observations at 1 km, while the mean Doppler velocity again matches the lower range of measurements but not the peaks. ZPIA estimates R similar to ZvPIA in this

regime, but without mean Doppler velocity in the lightest rain, fewer larger drops are retrieved with N_w tending toward the prior in some profiles. In contrast, Zv is very similar to ZvPIA in the lightest profiles with N_w consistently around $10^9\ m^{-4}$.

In warm rain we have retrieved N_w several orders of magnitude greater than the Marshall–Palmer value with D_0 in the range 0.1–0.5 mm in rain rates from very light drizzle up to $10\ mm\ h^{-1}$ in the heaviest profiles. The contribution of PIA and mean Doppler velocity to $R - N_w$ retrievals in warm rain differs from that in rain from melting ice: while Doppler is required to retrieve N_w when attenuation is low, it is possible to retrieve N_w without Doppler in strongly attenuated profiles of warm cloud where the combination of low radar reflectivity and high attenuation can only be due to a high concentration of small drops.

5 Dual-frequency radar retrievals

ER-2 aircraft measurements from TC4 provide a rare opportunity for airborne observations with multiple Doppler radars. In this study we have primarily used the 9.6 GHz radar to evaluate retrievals made with the 94 GHz radar; however, we can also use the dual-frequency radar measurements to exploit the different scattering behaviours and retrieve additional information about the DSD. Dual-frequency ratio (DFR) and differential Doppler velocity (DDV) techniques were applied to retrievals from ER-2 measurements during the CRYSTAL-FACE field experiment over Florida in 2002 (Liao et al., 2008, 2009), and Tian et al. (2007) exploited dual-frequency Doppler radar to retrieve rain DSD and vertical air motion for light stratiform rain from the same experiment. The CAPTIVATE framework can combine information from two radars by resolving differential non-Rayleigh scattering and mean Doppler velocities from multiple wavelengths.

We compare the dual-frequency radar retrievals with and without mean Doppler velocity measurements against the ZvPIA 94 GHz retrieval for Case 1, which covered a wide range of rain intensities, including a region in which the 94 GHz radar was fully attenuated (Fig. 13). The dual-frequency radar retrieval estimates of R are consistent with those from 94 GHz, with the exception of the non-Doppler dual-frequency radar retrieval in light rain where a high concentration of small drops is estimated, leading to an overestimate of R; in much of the lightest rain the hydrometeors may be below the sensitivity of the 9.6 GHz instrument, so the dual-frequency radar retrieval tends toward that from the 94 GHz radar. In the heavy shower where the ZvPIA estimates of Z have large uncertainties and N_w is very poorly constrained due to complete extinction of the 94 GHz radar beam, the dual-frequency radar retrievals use 9.6 GHz measurements alone to estimate R at around $10\ mm\ h^{-1}$; N_w remains in the range 10^6–$10^7\ m^{-4}$ as in the surrounding moderate rain, and D_0 is estimated between 1 and 2 mm. While the 94 GHz retrieval was capable of a cautious estimate of R with large retrieval uncertainty based on the gradient of radar reflectivity and saturated PIA, estimates of N_w cannot be justified when the radar is fully attenuated. The greatest errors in the non-Doppler dual-frequency radar retrieval are in forward-modelled Doppler velocity for the evaporating moderate rain profiles between 15:58 and 16:00 UTC where a higher concentration of smaller drops is retrieved; in this circumstance the addition of mean Doppler velocity leads to a stronger retrieval than a second radar wavelength. Overall the close agreement of the 94 GHz Doppler radar retrievals with the dual-frequency Doppler retrieval is a promising result, indicating that a single-frequency Doppler radar is sufficient for a retrieval of R and N_w within the limits of radar attenuation.

6 Retrieving vertical profiles of N_w

We have demonstrated the retrieval of rain rate as a function of both D_0 and N_w by making the simplifying assumption that N_w is constant with height in each profile. This is a significant improvement over retrievals in which N_w is assumed constant everywhere and retrieved values of N_w ranged over more than 5 orders of magnitude between light rain from melting ice and warm rain from liquid clouds; however, evaluation against 9.6 GHz radar measurements has shown that features within the vertical profile are not always accurately resolved with significant errors near the surface in cases where microphysical processes modify the DSD with height.

It is therefore of interest to represent N_w as varying through the vertical profile; however, there are limits to the degrees of freedom that can be retrieved with the available observed variables. In this section we explore the potential for one additional degree of freedom by allowing each profile of N_w to be represented by a linear gradient, as explored in Rose and Chandrasekar (2006) for a dual-frequency retrieval. Here the state vector becomes

$$\boldsymbol{x} = \ln\left[R_1 \cdots R_n \quad \overline{N_w} \quad N_w'\right]^T, \tag{12}$$

where $\overline{N_w}$ is the average N_w through the profile and N_w' is the gradient with height.

A retrieval in which N_w is represented by a linear profile (linear-N_w) is compared against the constant-N_w ZvPIA retrieval using the average profiles of retrieved and forward-modelled variables for a ZvPIA retrieval of moderate warm rain from Case 3 (Fig. 14). The linear-N_w retrieval significantly improves the fit with 94 GHz observed variables below 1.5 km where the constant-N_w retrieval underestimates mean Doppler velocity. The linear-N_w retrieval is also better able to forward model the independent 9.6 GHz radar variables with near-surface errors in mean Doppler velocity significantly reduced. The linear-N_w retrieval resolves a gradient in N_w from around $10^{11}\ m^{-4}$ at cloud top to $10^9\ m^{-4}$ near

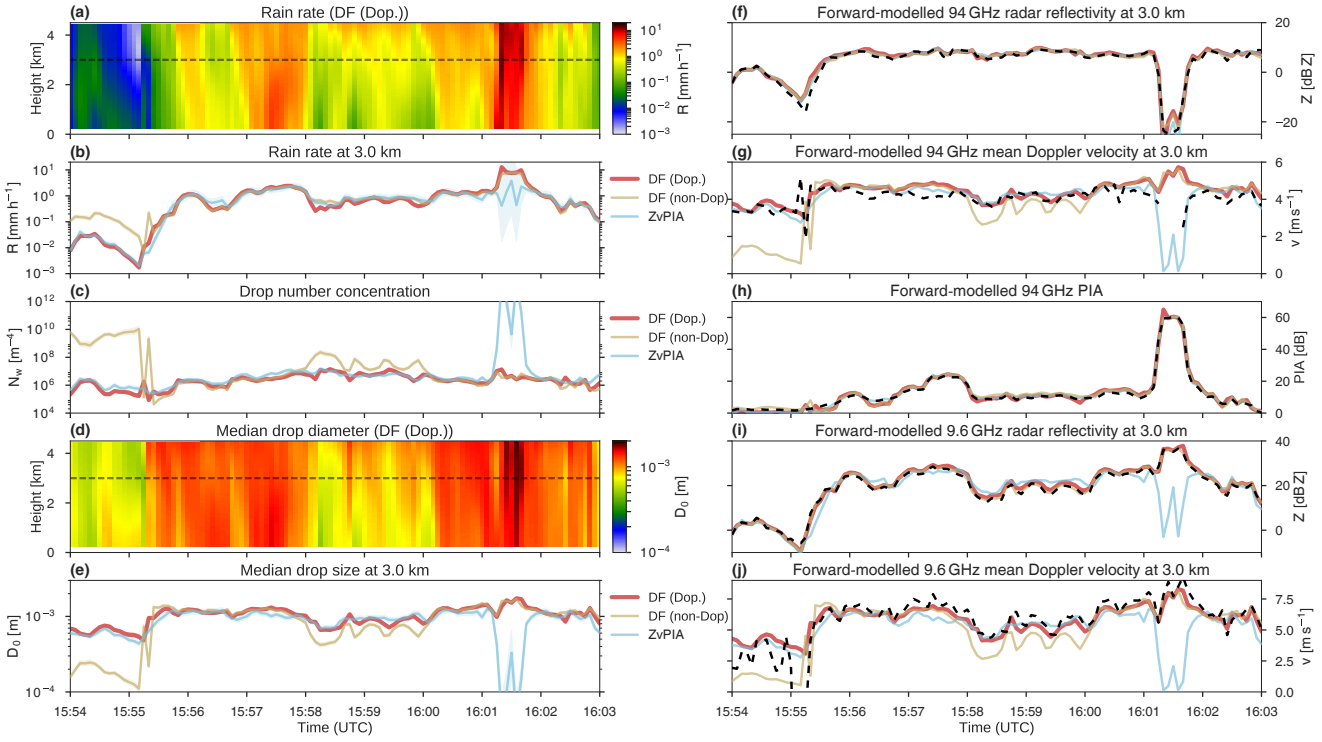

Figure 13. Time series of dual-frequency (DF) retrievals with and without Doppler compared against the 94 GHz ZvPIA retrieval for Case 1 on 22 July 2007. Retrieved state and derived variables **(a–e)** and forward-modelled radar measurements **(f–j)** for the three retrievals are shown at a height of 3.0 km a.s.l. (indicated with a light dashed line in the left-hand scenes), while the full scenes of R **(a)** and D_0 **(d)** are shown for the dual-frequency Doppler retrieval. Shading indicates the 1σ uncertainty in the retrieved and derived variables. Dark dashed lines **(f–j)** indicate the observed radar measurements.

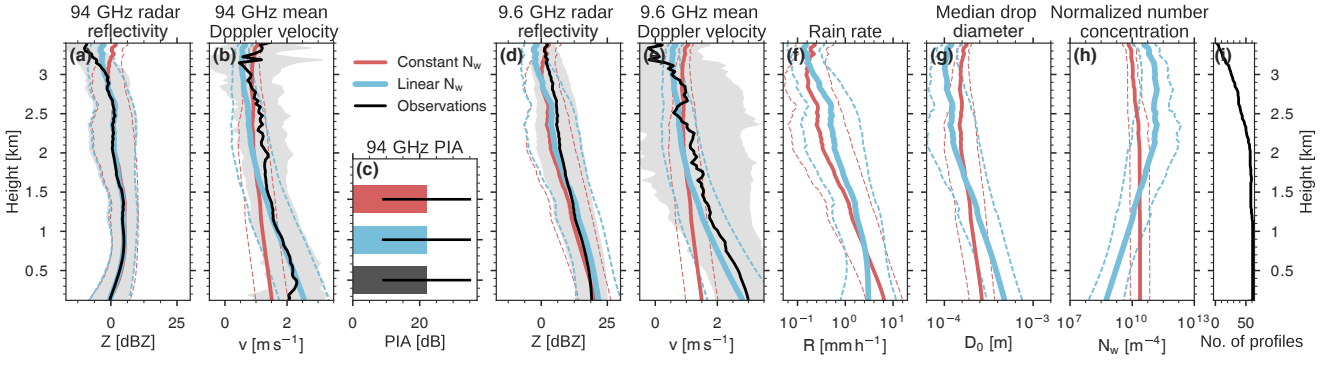

Figure 14. Averaged profiles of moderate rain between 12:41 and 12:46 UTC on 29 July 2007. Forward-modelled 94 GHz radar reflectivity **(a)**, mean Doppler velocity **(b)**, and PIA **(c)**; forward-modelled 9.6 GHz radar reflectivity **(d)** and mean Doppler velocity **(e)**; and retrieved rain rate **(f)**, median drop size **(g)**, and drop number concentration parameter **(h)** for ZvPIA retrievals in which N_w is represented as a constant with height and as a linear gradient. The number of profiles included at each height is indicated in **(i)**. Shading and dashed lines indicate the 1σ standard deviation of the retrieved and derived variables.

the surface and a steeper gradient of D_0, increasing from almost 0.1 mm near cloud top to around 0.5 mm at the surface. The changes in D_0 and N_w through the vertical profile have compensating effects on the profile of rain rate with the retrieved R increasing somewhat above 2 km and decreasing below 0.5 km by around a factor of 2.

With an additional degree of freedom the linear-N_w retrieval from 94 GHz radar exhibited increased variability in profiles in retrieved variables, suggesting that the problem is marginally constrained; for this reason it may not always be appropriate to make a linear-N_w retrieval with a single radar frequency. A dual-frequency linear-N_w retrieval esti-

mated substantially similar profiles of N_w and D_0 for the same case, indicating that the retrieved variation in the DSD with height is a robust feature when better constrained by additional observations. The retrieval of a linear gradient of N_w leads to an improved representation of warm rain, both as evaluated against independent 9.6 GHz radar variables and in that the retrieved profiles of N_w and D_0 qualitatively meet expectations for collision and coalescence processes. While this is a promising result, we note that the profile of R retrieved with linear N_w is substantially similar to that retrieved with a height-invariant representation of N_w and that the latter is better constrained by the measurements available to a retrieval from a 94 GHz Doppler radar.

7 Discussion and conclusions

The upcoming ESA/JAXA EarthCARE satellite will include a 94 GHz cloud-profiling radar, the first Doppler radar in space. In this study we have used an airborne 94 GHz Doppler radar to investigate the prospects for making improved rain retrievals by assimilating mean Doppler velocity measurements with a focus on improving upon radar rain retrievals from CloudSat in two key respects: (1) to facilitate rain rate estimates over land and (2) to reduce uncertainties in rain rate estimates by retrieving an additional parameter of the raindrop size distribution (DSD). Retrievals over a range of stratiform rain regimes were made from the 94 GHz Doppler radar aboard the ER-2 aircraft during the TC4 field campaign over the tropical Pacific in 2007 and evaluated against simultaneous measurements from the less attenuated 9.6 GHz Doppler radar.

The CAPTIVATE algorithm has been developed for the retrieval of rain, cloud, and aerosols from the synergy of active and passive instruments from EarthCARE; within the variational scheme multiple observational variables can be combined as available, and the retrieved variables and their physical representation can be configured at runtime. It is therefore possible with CAPTIVATE to combine the information from multiple airborne instruments, and the variational scheme allows uncertainties in the retrieved variables to be estimated from errors in the measurements and forward models.

The ambiguities of rain rate retrievals at strongly attenuated radar frequencies can be resolved by either an estimate of PIA or by the profile of mean Doppler velocity, which relates to drop size and is not affected by partial attenuation of the radar beam. The latter measurement has potential applications to making estimates of rain rate over land where PIA is more difficult to estimate from the surface backscatter. With both PIA and mean Doppler velocity it is possible to retrieve the rain rate as a function of two parameters of the DSD, median drop size D_0, and drop number concentration N_w. This improves upon significant uncertainties in previous rain rate estimation algorithms in which N_w is assumed constant everywhere.

Rain rate R and drop number concentration N_w were retrieved from airborne 94 GHz radar measurements of tropical stratiform rain over the ocean. The three cases covered a range of rain rates from virga to heavy showers from melting ice and liquid clouds. The 94 GHz radar was fully attenuated in profiles with rain rates up to 10 mm h^{-1} below a melting layer above 4 km and in rain from liquid clouds with tops around 3 km. The attenuation of the 94 GHz radar places an upper limit on the rain profiles that can be retrieved; however, we note that in the mid-latitudes where the melting layer is lower, it may be possible to make retrieval up to higher rain rates before the radar is fully attenuated. Retrievals were evaluated by forward modelling the 9.6 GHz measurements and comparing against independent measurements at that frequency; dual-frequency retrievals of rain rate were consistent with those derived from 94 GHz radar alone, except where that instrument was fully attenuated in moderate to heavy rain. Retrieved values of N_w were within the expected range of values for the respective rain regimes, ranging from 10^5 m^{-4} in light rain from melting ice (with D_0 around 1.0–1.5 mm) up to N_w of 10^{10} m^{-4} in moderate rain from liquid cloud (D_0 was around 0.1–0.3 mm); however, further work is required to evaluate retrieved rain DSD against in situ measurements.

In many contexts microphysical processes such as collision–coalescence, evaporation, and break-up are expected to modify the DSD through the vertical profile. With N_w assumed constant with height it was broadly possible to represent the major features of the vertical profile of independent 9.6 GHz radar measurements, but errors in the gradient of mean Doppler velocity indicated that the effects of evaporation or collision–coalescence were not resolved. We demonstrated that the 94 GHz Doppler radar measurements are sufficient to retrieve a linear gradient representation of N_w: in warm rain a decrease in drop concentration and an increase in drop size toward the surface were retrieved, which is consistent with expected effects of collision–coalescence processes in warm rain, leading to improved errors with respect to forward-modelled 9.6 GHz radar measurements. The retrieval of a linear profile of N_w has potential applications to both single- and multiple-frequency retrievals of precipitation (e.g. Rose and Chandrasekar, 2006) but must be well constrained by sufficient observational variables.

In combination with PIA, mean Doppler velocity provides sufficient information to make robust retrievals of R and N_w across a range of rain regimes. In light rain with negligible PIA, mean Doppler velocity provides sufficient constraint, suggesting the possibility of using Doppler radar for retrievals of light rain over land; however, in moderate rain rates PIA provides a necessary constraint on the rain rate. Satisfactory retrievals of rain rate over land may be achieved by assuming that N_w is constant, especially for cold stratiform rain; alternatively, PIA could be estimated from the land surface as in Iguchi et al. (2009), which may provide sufficient information to resolve the ambiguity between weakly

and strongly attenuating profiles even with large observational uncertainties. A robust method of using Doppler radar to estimate rain rate over land will be the subject of future work.

While Doppler velocity is generally required to retrieve N_w, in moderate warm rain from liquid clouds the combination of low radar reflectivity and strong radar attenuation was sufficient to retrieve the high concentration of small drops typical of warm rain without the need for Doppler velocity information. This finding may be applicable to retrievals of the drop number concentration in warm rain observed by CloudSat.

Airborne Doppler radar measurements contribute critical drop size information to improved estimates of the intensity and DSD of rain. Future work will focus on understanding the application of this retrieval methodology to space-borne Doppler radar, including the effects of multiple scattering and non-uniform beam filling on the Doppler measurements. With the first Doppler radar in space, EarthCARE stands to make improved global estimates of rain rate and drop size, providing new insights into the interactions of clouds and precipitation through the atmospheric profile.

Data availability. The ER-2 data from TC4 used in this study can be accessed via the NASA Earth Science Project Office (https://espo.nasa.gov/tc4). Alternatively, for data access and support, contact Lin Tian (lin.tian-1@nasa.gov) for ER-2 radar data and Dennis Hlavka (dennis.l.hlavka@nasa.gov]) for ER-2 lidar data. ERA-Interim data are available from ECMWF (http://apps.ecmwf.int/datasets/).

Competing interests. The authors declare that they have no conflict of interest.

Acknowledgements. This work was supported by the National Centre for Earth Observation (NCEO) and European Space Agency grant 4000112030/15/NL/CT with computing resources provided by the University of Reading. L. Tian's research is supported by NASA Precipitation Measurement Mission and Remote Sensing Theory. We thank Gerry Heymsfield and the ER-2 radar engineers for collecting CRS and EDOP data, Dennis Hlavka (NASA-GSFC) for assistance with CPL data, and Stephen Platnick and Howard Tan (NASA-JPL) for assistance with MAS/MASTER radiometer data. ERA-Interim data are produced and distributed by ECMWF and hosted by the Centre for Environmental Data Analysis.

We are grateful to Alain Protat and two anonymous referees for their constructive feedback and Ross Bannister, Nancy Nichols, Lars Isaksen, Elias Holm, and Mike Rennie for helpful discussions.

Edited by: Timothy J. Dunkerton
Reviewed by: Alain Protat and two anonymous referees

References

Abel, S. J. and Boutle, I. A.: An improved representation of the raindrop size distribution for single-moment microphysics schemes, Q. J. Roy. Meteorol. Soc., 138, 2151–2162, https://doi.org/10.1002/qj.1949, 2012.

Atlas, D., Srivastava, R., and Sekhon, R.: Doppler radar characteristics of precipitation at vertical incidence, Rev. Geophys., 11, 1–35, https://doi.org/10.1029/RG011i001p00001, 1973.

Battaglia, A. and Tanelli, S.: DOMUS: DOppler MUltiple-Scattering Simulator, IEEE T. Geosci. Remote, 49, 442–450, https://doi.org/10.1109/TGRS.2010.2052818, 2011.

Battaglia, A., Ajewole, M. O., and Simmer, C.: Multiple scattering effects due to hydrometeors on precipitation radar systems, Geophys. Res. Lett., 32, L19801, https://doi.org/10.1029/2005GL023810, 2005.

Battaglia, A., Ajewole, M. O., and Simmer, C.: Evaluation of radar multiple scattering effects in Cloudsat configuration, Atmos. Chem. Phys., 7, 1719–1730, https://doi.org/10.5194/acp-7-1719-2007, 2007.

Beard, K. V.: Terminal Velocity and Shape of Cloud and Precipitation Drops Aloft, J. Atmos. Sci., 33, 851–864, https://doi.org/10.1175/1520-0469(1976)033<0851:TVASOC>2.0.CO;2, 1976.

Behrangi, A., Lebsock, M., Wong, S., and Lambrigtsen, B.: On the quantification of oceanic rainfall using space-borne sensors, J. Geophys. Res.-Atmos., 117, D20105, https://doi.org/10.1029/2012JD017979, 2012.

Berg, W., L'Ecuyer, T., Haynes, J. M., Berg, W., L'Ecuyer, T., and Haynes, J. M.: The Distribution of Rainfall over Oceans from Spaceborne Radars, J. Appl. Meteorol. Clim., 49, 535–543, https://doi.org/10.1175/2009JAMC2330.1, 2010.

Ceccaldi, M., Delanoë, J., Hogan, R. J., Pounder, N. L., Protat, A., and Pelon, J.: From CloudSat-CALIPSO to EarthCare: Evolution of the DARDAR cloud classification and its comparison to airborne radar-lidar observations, J. Geophys. Res.-Atmos., 118, 7962–7981, https://doi.org/10.1002/jgrd.50579, 2013.

Dee, D. P., Uppala, S. M., Simmons, A. J., Berrisford, P., Poli, P., Kobayashi, S., Andrae, U., Balmaseda, M. A., Balsamo, G., Bauer, P., Bechtold, P., Beljaars, A. C. M., van de Berg, L., Bidlot, J., Bormann, N., Delsol, C., Dragani, R., Fuentes, M., Geer, A. J., Haimberger, L., Healy, S. B., Hersbach, H., Hólm, E. V., Isaksen, L., Kållberg, P., Köhler, M., Matricardi, M., McNally, A. P., Monge-Sanz, B. M., Morcrette, J. J., Park, B. K., Peubey, C., de Rosnay, P., Tavolato, C., Thépaut, J. N., and Vitart, F.: The ERA-Interim reanalysis: configuration and performance of the data assimilation system, Q. J. Roy. Meteorol. Soc., 137, 553–597, https://doi.org/10.1002/qj.828, 2011.

Firda, J. M., Sekelsky, S. M., McIntosh, R. E., Firda, J. M., Sekelsky, S. M., and McIntosh, R. E.: Application of Dual-Frequency Millimeter-Wave Doppler Spectra for the Retrieval of Drop Size Distributions and Vertical Air Motion in Rain, J. Atmos. Ocean. Tech., 16, 216–236, https://doi.org/10.1175/1520-0426(1999)016<0216:AODFMW>2.0.CO;2, 1999.

Frisch, A. S., Fairall, C. W., and Snider, J. B.: Measurement of Stratus Cloud and Drizzle Parameters in ASTEX with a $K\alpha$-Band Doppler Radar and a Microwave Radiometer, J. Atmos. Sci., 52, 2788–2799, https://doi.org/10.1175/1520-0469(1995)052<2788:MOSCAD>2.0.CO;2, 1995.

Hawkness-Smith, L.: A novel retrieval of liquid water path and a evaluation of the representation of drizzle in numerical models, PhD thesis, University of Reading, Reading, http://ethos.bl.uk/OrderDetails.do?uin=uk.bl.ethos.533772 (last access: 19 January 2017), 2010.

Haynes, J. M., L'Ecuyer, T. S., Stephens, G. L., Miller, S. D., Mitrescu, C., Wood, N. B., and Tanelli, S.: Rainfall retrieval over the ocean with spaceborne W-band radar, J. Geophys. Res., 114, D00A22, https://doi.org/10.1029/2008JD009973, 2009.

Haynes, J. M., Jakob, C., Rossow, W. B., Tselioudis, G., and Brown, J. R.: Major Characteristics of Southern Ocean Cloud Regimes and Their Effects on the Energy Budget, J. Climate, 24, 5061–5080, https://doi.org/10.1175/2011JCLI4052.1, 2011.

Heymsfield, G. M., Bidwell, S. W., Caylor, I. J., Ameen, S., Nicholson, S., Boncyk, W., Miller, L., Vandemark, D., Racette, P. E., and Dod, L. R.: The EDOP Radar System on the High-Altitude NASA ER-2 Aircraft, J. Atmos. Ocean. Tech., 13, 795–809, https://doi.org/10.1175/1520-0426(1996)013<0795:TERSOT>2.0.CO;2, 1996.

Hitschfeld, W. and Bordan, J.: Errors inherent in the radar measurement of rainfall at attenuating wavelengths, J. Meteorol., 11, 58–67, https://doi.org/10.1175/1520-0469(1954)011<0058:EIITRM>2.0.CO;2, 1954.

Hogan, R. J.: A Variational Scheme for Retrieving Rainfall Rate and Hail Reflectivity Fraction from Polarization Radar, J. Appl. Meteorol. Clim., 46, 1544–1564, https://doi.org/10.1175/JAM2550.1, 2007.

Hogan, R. J.: Fast Lidar and Radar Multiple-Scattering Models. Part I: Small-Angle Scattering Using the Photon Variance-Covariance Method, J. Atmos. Sci., 65, 3621–3635, https://doi.org/10.1175/2008JAS2642.1, 2008.

Hook, S. J. S., Myers, J. J. J., Thome, K. K. J., Fitzgerald, M., and Kahle, A. B.: The MODIS/ASTER airborne simulator (MASTER) – a new instrument for earth science studies, Remote Sens. Environ., 76, 93–102, https://doi.org/10.1016/S0034-4257(00)00195-4, 2001.

Hou, A. Y., Kakar, R. K., Neeck, S., Azarbarzin, A. A., Kummerow, C. D., Kojima, M., Oki, R., Nakamura, K., Iguchi, T., Hou, A. Y., Kakar, R. K., Neeck, S., Azarbarzin, A. A., Kummerow, C. D., Kojima, M., Oki, R., Nakamura, K., and Iguchi, T.: The Global Precipitation Measurement Mission, B. Am. Meteorol. Soc., 95, 701–722, https://doi.org/10.1175/BAMS-D-13-00164.1, 2014.

Iguchi, T., Kozu, T., Meneghini, R., Awaka, J., Okamoto, K., Iguchi, T., Kozu, T., Meneghini, R., Awaka, J., and Okamoto, K.: Rain-Profiling Algorithm for the TRMM Precipitation Radar, J. Appl. Meteorol., 39, 2038–2052, https://doi.org/10.1175/1520-0450(2001)040<2038:RPAFTT>2.0.CO;2, 2000.

Iguchi, T., Kozu, T., Kwaitkowski, J., Meneghini, R., Awaka, J., and Okamoto, K.: Uncertainties in the Rain Profiling Algorithm for the TRMM Precipitation Radar, J. Meteorol. Soc. Jpn., 87A, 1–30, https://doi.org/10.2151/jmsj.87A.1, 2009.

Illingworth, A. J. and Blackman, T. M.: The Need to Represent Raindrop Size Spectra as Normalized Gamma Distributions for the Interpretation of Polarization Radar Observations, J. Appl. Meteorol., 41, 286–297, https://doi.org/10.1175/1520-0450(2002)041<0286:TNTRRS>2.0.CO;2, 2002.

Illingworth, A. J., Barker, H. W., Beljaars, A., Ceccaldi, M., Chepfer, H., Clerbaux, N., Cole, J., Delanoë, J., Domenech, C., Donovan, D. P., Fukuda, S., Hirakata, M., Hogan, R. J., Huenerbein, A., Kollias, P., Kubota, T., Nakajima, T., Nakajima, T. Y., Nishizawa, T., Ohno, Y., Okamoto, H., Oki, R., Sato, K., Satoh, M., Shephard, M. W., Velázquez-Blázquez, A., Wandinger, U., Wehr, T., and van Zadelhoff, G.-J.: The EarthCARE Satellite: The Next Step Forward in Global Measurements of Clouds, Aerosols, Precipitation, and Radiation, B. Am. Meteorol. Soc., 96, 1311–1332, https://doi.org/10.1175/BAMS-D-12-00227.1, 2015.

King, M. D., Menzel, W. P., Grant, P. S., Myers, J. S., Arnold, G. T., Platnick, S. E., Gumley, L. E., Tsay, S.-C., Moeller, C. C., Fitzgerald, M., Brown, K. S., Osterwisch, F. G., King, M. D., Menzel, W. P., Grant, P. S., Myers, J. S., Arnold, G. T., Platnick, S. E., Gumley, L. E., Tsay, S.-C., Moeller, C. C., Fitzgerald, M., Brown, K. S., and Osterwisch, F. G.: Airborne Scanning Spectrometer for Remote Sensing of Cloud, Aerosol, Water Vapor, and Surface Properties, J. Atmos. Ocean. Tech., 13, 777–794, https://doi.org/10.1175/1520-0426(1996)013<0777:ASSFRS>2.0.CO;2, 1996.

Kollias, P., Rémillard, J., Luke, E., and Szyrmer, W.: Cloud radar Doppler spectra in drizzling stratiform clouds: 1. Forward modeling and remote sensing applications, J. Geophys. Res., 116, D13201, https://doi.org/10.1029/2010JD015237, 2011a.

Kollias, P., Szyrmer, W., Rémillard, J., and Luke, E.: Cloud radar Doppler spectra in drizzling stratiform clouds: 2. Observations and microphysical modeling of drizzle evolution, J. Geophys. Res., 116, D13203, https://doi.org/10.1029/2010JD015238, 2011b.

Kummerow, C., Barnes, W., Kozu, T., Shiue, J., Simpson, J., Kummerow, C., Barnes, W., Kozu, T., Shiue, J., and Simpson, J.: The Tropical Rainfall Measuring Mission (TRMM) Sensor Package, J. Atmos. Ocean. Tech., 15, 809–817, https://doi.org/10.1175/1520-0426(1998)015<0809:TTRMMT>2.0.CO;2, 1998.

Lebsock, M. D. and L'Ecuyer, T. S.: The retrieval of warm rain from CloudSat, J. Geophys. Res.-Atmos., 116, D20209, https://doi.org/10.1029/2011JD016076, 2011.

Lebsock, M. D., L'Ecuyer, T. S., and Stephens, G. L.: Detecting the Ratio of Rain and Cloud Water in Low-Latitude Shallow Marine Clouds, J. Appl. Meteorol. Clim., 50, 419–432, https://doi.org/10.1175/2010JAMC2494.1, 2011.

Lebsock, M. D., Morrison, H., and Gettelman, A.: Microphysical implications of cloud-precipitation covariance derived from satellite remote sensing, J. Geophys. Res.-Atmos., 118, 6521–6533, https://doi.org/10.1002/jgrd.50347, 2013.

L'Ecuyer, T. S. and Stephens, G. L.: An Estimation-Based Precipitation Retrieval Algorithm for Attenuating Radars, J. Appl. Meteorol., 41, 272–285, https://doi.org/10.1175/1520-0450(2002)041<0272:AEBPRA>2.0.CO;2, 2002.

Li, L., Heymsfield, G. M., Racette, P. E., Tian, L., and Zenker, E.: A 94-GHz Cloud Radar System on a NASA High-Altitude ER-2 Aircraft, J. Atmos. Ocean. Tech., 21, 1378–1388, https://doi.org/10.1175/1520-0426(2004)021<1378:AGCRSO>2.0.CO;2, 2004.

Liao, L., Meneghini, R., Tian, L., and Heymsfield, G. M.: Retrieval of Snow and Rain From Combined X- and W-Band Airborne Radar Measurements, IEEE T. Geosci. Remote, 46, 1514–1524, https://doi.org/10.1109/TGRS.2008.916079, 2008.

Liao, L., Meneghini, R., Tian, L., and Heymsfield, G. M.: Measurements and Simulations of Nadir-Viewing Radar Returns from the

Melting Layer at X and W Bands, J. Appl. Meteorol. Clim., 48, 2215–2226, https://doi.org/10.1175/2009JAMC2033.1, 2009.

Liebe, H. J.: An updated model for millimeter wave propagation in moist air, Radio Sci., 20, 1069–1089, https://doi.org/10.1029/RS020i005p01069, 1985.

Luke, E. P. and Kollias, P.: Separating Cloud and Drizzle Radar Moments during Precipitation Onset Using Doppler Spectra, J. Atmos. Ocean. Tech., 30, 1656–1671, https://doi.org/10.1175/JTECH-D-11-00195.1, 2013.

Mace, G. G., Avey, S., Cooper, S., Lebsock, M., Tanelli, S., and Dobrowalski, G.: Retrieving co-occurring cloud and precipitation properties of warm marine boundary layer clouds with A-Train data, J. Geophys. Res.-Atmos., 121, 4008–4033, https://doi.org/10.1002/2015JD023681, 2016.

Marshall, J. and Palmer, W.: The distribution of raindrops with size, J. Meteorol., 5, 165–166, https://doi.org/10.1175/1520-0469(1948)0053C0165:TDORWS3E2.0.CO;2, 1948.

Matrosov, S. Y.: Potential for attenuation-based estimations of rainfall rate from CloudSat, Geophys. Res. Lett., 34, L05817, https://doi.org/10.1029/2006GL029161, 2007.

Matrosov, S. Y.: Assessment of Radar Signal Attenuation Caused by the Melting Hydrometeor Layer, IEEE T. Geosci. Remote, 46, 1039–1047, https://doi.org/10.1109/TGRS.2008.915757, 2008.

McGill, M., Hlavka, D., Hart, W., Scott, V. S., Spinhirne, J., and Schmid, B.: Cloud Physics Lidar: instrument description and initial measurement results, Appl. Optics, 41, 3725, https://doi.org/10.1364/AO.41.003725, 2002.

McGill, M. J.: Combined lidar-radar remote sensing: Initial results from CRYSTAL-FACE, J. Geophys. Res., 109, D07203, https://doi.org/10.1029/2003JD004030, 2004.

Meneghini, R. and Liao, L.: Effective Dielectric Constants of Mixed-Phase Hydrometeors, J. Atmos. Ocean. Tech., 17, 628–640, https://doi.org/10.1175/1520-0426(2000)017<0628:EDCOMP>2.0.CO;2, 2000.

Meneghini, R., Eckerman, J., and Atlas, D.: Determination of Rain Rate from a Spaceborne Radar Using Measurements of Total Attenuation, IEEE T. Geosci. Remote, GE-21, 34–43, https://doi.org/10.1109/TGRS.1983.350528, 1983.

Mie, G.: Beiträge zur Optik trüber Medien, speziell kolloidaler Metallösungen, Annal. Physik, 330, 377–445, https://doi.org/10.1002/andp.19083300302, 1908.

Mishchenko, M. I., Travis, L. D., and Mackowski, D. W.: T-matrix computations of light scattering by nonspherical particles: A review, J. Quant. Spectrosc. Ra., 55, 535–575, https://doi.org/10.1016/0022-4073(96)00002-7, 1996.

Moisseev, D. N. and Chandrasekar, V.: Examination of the μ–Λ Relation Suggested for Drop Size Distribution Parameters, J. Atmos. Ocean. Tech., 24, 847–855, https://doi.org/10.1175/JTECH2010.1, 2007.

Nelson, E. L., L'Ecuyer, T. S., Saleeby, S. M., Berg, W., Herbener, S. R., van den Heever, S. C., Nelson, E. L., L'Ecuyer, T. S., Saleeby, S. M., Berg, W., Herbener, S. R., and v. d. Heever, S. C.: Toward an Algorithm for Estimating Latent Heat Release in Warm Rain Systems, J. Atmos. Ocean. Tech., 33, 1309–1329, https://doi.org/10.1175/JTECH-D-15-0205.1, 2016.

O'Connor, E. J., Hogan, R. J., and Illingworth, A. J.: Retrieving Stratocumulus Drizzle Parameters Using Doppler Radar and Lidar, J. Appl. Meteorol., 44, 14–27, https://doi.org/10.1175/JAM-2181.1, 2005.

Rapp, A. D., Lebsock, M., L'Ecuyer, T., and L'Ecuyer, T.: Low cloud precipitation climatology in the southeastern Pacific marine stratocumulus region using CloudSat, Environ. Res. Lett., 8, 014 027, https://doi.org/10.1088/1748-9326/8/1/014027, 2013.

Rodgers, C.: Inverse methods for atmospheric sounding: theory and practice, World Scientific, Hackensack, N.J., 2000.

Rose, C. R. and Chandrasekar, V.: A GPM Dual-Frequency Retrieval Algorithm: DSD Profile-Optimization Method, J. Atmos. Ocean. Tech., 23, 1372–1383, https://doi.org/10.1175/JTECH1921.1, 2006.

Stephens, G. L., Vane, D. G., Boain, R. J., Mace, G. G., Sassen, K., Wang, Z., Illingworth, A. J., O'Connor, E. J., Rossow, W. B., Durden, S. L., Miller, S. D., Austin, R. T., Benedetti, A., Mitrescu, C., and the CloudSat Science Team: The CloudSat mission and the A-Train, B. Am. Meteorol. Soc., 83, 1771–1790, 2002.

Stephens, G. L., L'Ecuyer, T., Forbes, R., Gettlemen, A., Golaz, J.-C., Bodas-Salcedo, A., Suzuki, K., Gabriel, P., and Haynes, J.: Dreary state of precipitation in global models, J. Geophys. Res., 115, D24211, https://doi.org/10.1029/2010JD014532, 2010.

Testud, J., Oury, S., Black, R. A., Amayenc, P., and Dou, X.: The Concept of "Normalized" Distribution to Describe Raindrop Spectra: A Tool for Cloud Physics and Cloud Remote Sensing, J. Appl. Meteorol., 40, 1118–1140, https://doi.org/10.1175/1520-0450(2001)040<1118:TCONDT>2.0.CO;2, 2001.

Thurai, M., Huang, G. J., Bringi, V. N., Randeu, W. L., Schönhuber, M., Thurai, M., Huang, G. J., Bringi, V. N., Randeu, W. L., and Schönhuber, M.: Drop Shapes, Model Comparisons, and Calculations of Polarimetric Radar Parameters in Rain, J. Atmos. Ocean. Tech., 24, 1019–1032, https://doi.org/10.1175/JTECH2051.1, 2007.

Tian, L., Heymsfield, G. M., Li, L., and Srivastava, R. C.: Properties of light stratiform rain derived from 10- and 94-GHz airborne Doppler radars measurements, J. Geophys. Res., 112, D11211, https://doi.org/10.1029/2006JD008144, 2007.

Tokay, A. and Short, D. A.: Evidence from Tropical Raindrop Spectra of the Origin of Rain from Stratiform versus Convective Clouds, J. Appl. Meteorol., 35, 355–371, https://doi.org/10.1175/1520-0450(1996)035<0355:EFTRSO>2.0.CO;2, 1996.

Toon, O. B. O., Starr, D. O. D., Jensen, E. J., Newman, P. A., Platnick, S., Schoeberl, M. R., Wennberg, P. O., Wofsy, S. C., Kurylo, M. J., Maring, H., Jucks, K. W., Craig, M. S., Vasques, M. F., Pfister, L., Rosenlof, K. H., Selkirk, H. B., Colarco, P. R., Kawa, S. R., Mace, G. G., Minnis, P., and Pickering, K. E.: Planning, implementation, and first results of the Tropical Composition, Cloud and Climate Coupling Experiment (TC4), J. Geophys. Res., 115, D00J04, https://doi.org/10.1029/2009JD013073, 2010.

Twomey, S.: Introduction to the Mathematics of Inversion in Remote Sensing and Indirect Measurements, Elsevier Scientific Publishing Co., Amsterdam, 1977.

Weston, P. P., Bell, W., and Eyre, J. R.: Accounting for correlated error in the assimilation of high-resolution sounder data, Q. J. Roy. Meteorol. Soc., 140, 2420–2429, https://doi.org/10.1002/qj.2306, 2014.

Wilson, D. R., Illingworth, A. J., Blackman, T. M., Wilson, D. R., Illingworth, A. J., and Blackman, T. M.: Differential Doppler Velocity: A Radar Parameter for Characterizing Hy-

drometeor Size Distributions, J. Appl. Meteorol., 36, 649–663, https://doi.org/10.1175/1520-0450-36.6.649, 1997.

Wood, R., Kubar, T. L., Hartmann, D. L., and Wood, R.: Understanding the Importance of Microphysics and Macrophysics for Warm Rain in Marine Low Clouds. Part II: Heuristic Models of Rain Formation, J. Atmos. Sci., 66, 2953–2972, https://doi.org/10.1175/2009JAS3072.1, 2009.

Yoshida, R., Okamoto, H., Hagihara, Y., and Ishimoto, H.: Global analysis of cloud phase and ice crystal orientation from Cloud-Aerosol Lidar and Infrared Pathfinder Satellite Observation (CALIPSO) data using attenuated backscattering and depolarization ratio, J. Geophys. Res., 115, D00H32, https://doi.org/10.1029/2009JD012334, 2010.

Zhang, G., Vivekanandan, J., and Brandes, E.: A method for estimating rain rate and drop size distribution from polarimetric radar measurements, IEEE T. Geosci. Remote, 39, 830–841, https://doi.org/10.1109/36.917906, 2001.